https://doi.org/10.5194/egusphere-2025-2378
Preprint. Discussion started: 27 June 2025

Global shifts in mountain wave turbulence within high resolution climate models.

Isabel H. Smith[1], Paul D. Williams[1], and Reinhard Schiemann[1,2]

[1]University of Reading, UK
[2]National Center for Atmospheric Sciences, UK

Correspondence: Isabel H. Smith (smith.isabel.helen@gmail.com)

Abstract. Using a multi-model approach, this paper quantified global changes in moderate or greater mountain wave turbulence (MWT) within a high-end warming scenario. Initial results found model resolution dependency apparent, therefore three high resolution global climate modelled datasets were used within the analysis; HadGEM3-GC3.1-HM (25km), EC-Earth-3P-HR(36km) and MPI-ESM1.2-XR (34km). Regional dependencies developed around each model and index, with seasonal components an important contributor to results. A sub-continental approach was developed, focusing on all regions in which MWT arose. On average, the North American continent projected an increase in MWT, but a decrease over the Rocky Mountain range. This decrease was apparent in all seasons but northern hemisphere (NH) winter, with an increase of +60.6% over the 101 year investigation period. NH summer, spring and autumn dropped by -58.3%, -41.2 % and -30.9%. Over several mountain ranges an increase was evident, particularly over Greenland and regions in Asia. However, a drop in MWT also arose over the Alps, Atlas and northern and central Andes. Southern Andes and the Himalayas had seasonal differences resulting in a mix of projected outcomes. A final aim arose around the connection to low-level, surface wind flow and MWT production. This paper found links between MWT trends and the shift in projected median surface wind flow. The aviation sector should be aware of the future projections in MWT, particularly for those were large increase over the 101 year period were evident, such as Asia, Greenland and the Antarctic.

1 Introduction

Mountains have a large impact on the atmosphere, from increasing localised precipitation events, to generating vertical and horizontal atmospheric waves. Mountain waves can grow, as they propagate into higher altitudes with lower air density (Kim et al., 2018), steepen and eventually overturn breaking down into turbulent flow. This breakdown develops typically lower at the tropopause. This boundary, between the troposphere and stratosphere, is a region of enhanced turbulent mixing, with ozone, water vapour and aerosols exchanged between both layers (Whiteway et al.,2003; lane et.al, 2009). This height is also a typical cruising altitude for the aircraft, a part of the flight in which passengers and on-board crew are more likely not to be wearing their seat belts (Kim et al., 2018). This type of upper level turbulence is referred to as Mountain Wave Turbulence (MWT). MWT is the most

https://doi.org/10.5194/egusphere-2025-2378
Preprint. Discussion started: 27 June 2025

significant mechanisms that impacts aircraft safety near mountains (Lane et al., 2009). Atmospheric turbulence has a dangerous and damaging cost on the aviation sector. Delays, injuries and fatalities have a huge economic loss worth millions of US dollars a year (Wolff and Sharman, 2008). An aircraft caught in a patch of turbulence has to quickly change altitude. This leads to substantial shift in airspeed, which increases the chance of a system stall (Sharman and Pearsons, 2017). Types of upper-level turbulence are defined by the features which develop them, for example turbulence that develops in vertically deep convective cloud is referred to convectively induced turbulence (CIT) (Wolf and Sharman 2008). MWT, unlike CIT, is not detectable by on-board RADAR equipment (Sharman and Lane, 2016). Therefore flights can be struck suddenly which can lead to serious injuries and damages. Clear Air Turbulence (CAT), coined due to its formation without any convective features, is also not delectable. CAT often forms in the presence of an upper level frontal system, a jet core or jet stream. MWT is often included within CAT, due to its cloud-free, stratified development.

Global troposheric warming has an impact on the frequency of CAT production in both observations and projected modeled data, with a global increase concluded in several studies (Williams and Joshi, 2013: Kim et al. 2023; Prosser et al., 2023; Storer et al. 2019 and Smith et al. 2023). Upper level jet streams are shifting in speed and momentum with global temperature gradients altered, resulting in an increase in CAT production. However, new areas of research are trying to quantify the impact of global warming on MWT. Any future change to MWT will be equated to a shift in low level wind speed or a change in upper-level dynamical features suppressing or energising the breaking of inertial gravity waves. Kim et al. (2023), using a high-end SSP climate scenario, investigated the change in MWT between 1970-2014 and 2056-2101. Their paper used 14 different diagnostics to represent MWT within model data, with several indices and regions projecting an increase in the probability of encountering strong turbulence. The regions with a decline in MWT, had near-surface winds projected to also weaken in time. Observations have shown a global slowing in surface winds over previous decades, refereed to in literature as terrestrial stilling (TS). Despite TS shifting with several modes of climate variability (Zeng et al, 2019), it is projected to continue in many areas of the globe, including the northern hemisphere (NH) mid latitudes, in both middle to high warming projections (Deng et al., 2022). Kim et al. (2023) overall found an increase in MWT over two thirds of the globe, with large variations over the tropical regions.

Aircraft encountering turbulence are required to record the time, location and severity of the event. These reports are referred to as PIREPs. PIREP datasets are effective for turbulent climatology research but are not always reliable in their location or timing (Gill,2018), with median uncertainties of around 50km horizontally, 70m vertically and 200s temporally out (Sharman et al., 2006). Many previous studies, investigating trends in atmospheric turbulence, have used global climate models (GCMs) over PIREPs. Williams ands Storer (2022) found GCMs can effectively represent turbulence in the atmosphere as well as re-analysis data. The latest phase of the Coupled Model Intercomparison Project (CMIP6) has a subsection of high resolution global climate models (HighResMIP). This subsection was developed to bridge the gap between numerical weather predictions grid spacing sizes and GCMs, and to investigate global meteorological dynamical processes in higher resolution (Haarsma et al. 2016; Smith, et al.. 2023). This paper

https://doi.org/10.5194/egusphere-2025-2378
Preprint. Discussion started: 27 June 2025

aims to understand if MWT is projected to change within CMIP6 HighResMIP models over a 101 year period starting in 1950 and ending in 2050, using some indices applied in Kim et. al (2023). Also, we aims to understand if resolution is important for capturing MWT, if CMIP6 models project TS and if TS differences globally result in changes to MWT. A final aim is to understand seasonality variation in MWT changes.

2 Methodology and Data

MWT is difficult to forecast, with the theory very well understood, but capacity to resolve the wave-length of inertial gravity waves and the turbulent kinetic energy difficult due to its small scale nature (Gill and Striling, 2013). One can assume large scale eddies will eventually cascade down the inertial sub-range into micro-scale sizes and into turbulent kinetic energy (Lester 1993, Sharman and Lane, 2016). This assumption allows investigations to use data with a range of resolutions. CMIP was set up in the 1990s to evaluate, collate and improve GCMs. Simulations from three CMIP6-HighResMIP GCMs are used in this study. These GCMs are HadGEM3-GC3.1, with three grid spacing domains available (-HM; 25km, -MM; 60km, -LL; 135km), MPI-ESM1.2 with two domains (-XR; 34km, -HR; 67km) and EC-Earth with two domains (-3P-HR; 36km , -3P; 71km). The finer sub-models may start to resolve patches of turbulence, which are 60km wide and 1km deep (Sharman et al., 2014).

To diagnose regions of turbulence, a number of indices, linked closely to atmospheric instability, are applied to our CMIP6 GCMs data. MWT and CAT share similarities in their formation, so previous literature has applied CAT indices to represent MWT in the atmosphere. Sharman and Pearsons (2017) and Kim et al.(2023) combine CAT diagnostics with certain surface and terrain variables to create an index that just diagnoses MWT;

$$Index_{MWT} = Index_{CAT} * Ds$$

Ds is the near-surface element. Within this paper, Ds = surface height (>200m) multiplied by both terrain gradient (>0.5 km m^{-1}) and surface wind speed. Sharman and Pearsons (2017) determined, through experimentation, that these three variables within Ds combined with a CAT diagnostics represented MWT effectively. Kim et al. (2023) tested using vertical velocity within Ds, instead of low-level wind speed, but found a poorer statistical evaluation. Terrain gradient is an important quantity with its association with linear gravity wave theory, and the wave of a gravity wave amplitude being proportional to the terrain slope magnitude (Wolf and Sharman, 2008). This method of calculating MWT was deemed skilful against PIREP data, in comparison to a orthographic gravity wave parametrisation scheme (Kim et al., 2018). In our study, we apply six indices used previously to diagnose the presence of CAT (Williams, Joshi (2014). These CAT indices are Horizontal temperature gradient (HTG), Frontogensis function (FF), the divergence of horizontal wind (DIV), wind speed (WS), flow deformation (FD) and finally a combination of flow deformation and wind speed (FDWS). Each MWT index is denoted with the subscript of their CAT index contributions, for example MWT_{HTG} is the product of Horizontal temperature Gradient and Ds. Sharman and Pearsons (2017) found that these 6 indices, with 8 others, are very well at representing MWT at high

https://doi.org/10.5194/egusphere-2025-2378
Preprint. Discussion started: 27 June 2025

altitudes with an area under the curve (AUC) of 0.989 within Receiving operating curve (ROC) analysis. Horizontal Temperature gradient (combined with Ds) also was found to pick up MWT effectively with an AUC of 0.991. These results have only been tested over the contiguous united states of America (CONUS). Our study assumes moderate or greater (MOG) turbulence is arising globally at the 98th percentile value of each index, following recent MWT literature (Kim et al., 2023) and focuses on the atmospheric pressure of 200 hPa.

Low-level wind speed is a variable considered on its own within this paper. The variations in the maximum and median values in wind speed are investigated separately. This method was determined to understand on average how surface wind flow is changing, and if this change is also found in the high-end maximum wind flow.

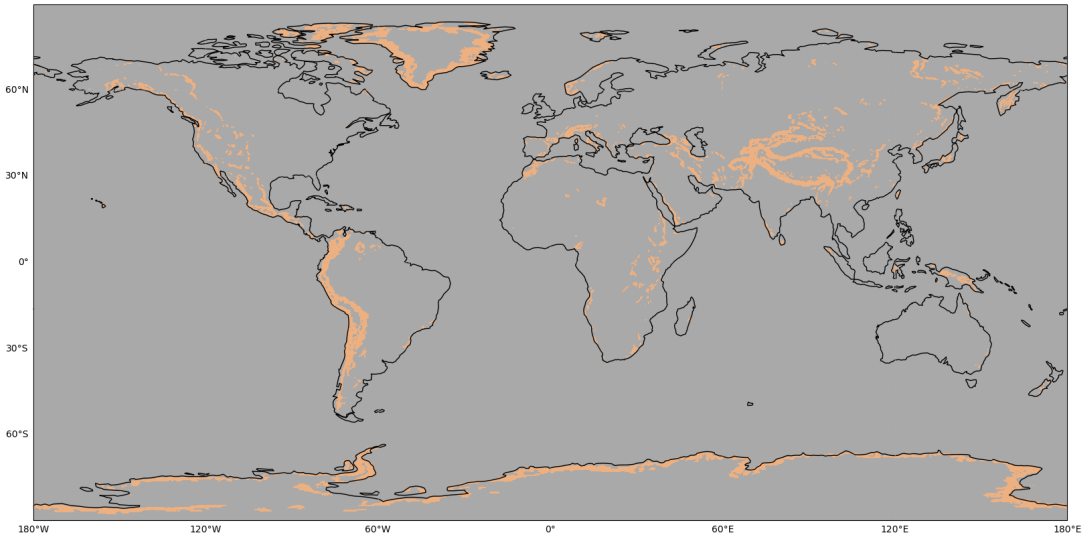

Figure 1. Areas of the globe in which our GCMs project MWT, averaged over three GCMs; HadGEM3-GC3.1-HM, MPI-ESM1.2-XR and EC-Earth-3P-HR, across all indices; MWT_{FD}, MWT_{FDWS},MWT_{WS}, MWT_{HTG}, MWT_{FF},MWT_{DIV}.

3 Results and Discussion

As discussed, terrain height and gradient are applied to CAT indices to identify MWT. The importance of terrain gradient is highlighted effectively in figure 1. This figure shows the regions of the globe where our indices diagnose MWT. Regions of the globe with large plateaus, such as Greenland and the Tibetan Plateau, are enclosed by areas of MWT with these steep slopes dominating. As expected, MWT is most prominent over large mountain ranges, such as the Andes, Rocky and Himalayas.

https://doi.org/10.5194/egusphere-2025-2378
Preprint. Discussion started: 27 June 2025

3.1 Two Decade Comparison

The MOG MWT decadal difference between 1950-60 and 2040-50 are displayed within figure 2 . Here this relative change in MWT is shown for all models domain sizes averaged across the six indices. A definitive lack of detail is evident within mid-range/coarser sub-models, clearly shown by HadGEM3-GC3.1-LL (figure 2i) with few MWT zones. Previous PIREP analysis suggests that there are considerable more regions where aircraft have experienced MWT, for example North America projected MWT is non-existent within this 135km grid spaced model. For MWT, a resolution dependence has arisen. Interestingly, the mid-range sub-models project similar MWT changes, when compared to their finer counterparts. This is shown effectively within subplots (2g) and (2h), which display the average across the models, regridded to 36km and 71km respectively. Both subplots have a separate steep increase or decrease over Greenland and northern South America. However, there are differences in the amount of "white" patches, which simply project "no-change" but the occurrence of MWT. The agreement across model resolutions, adds weight to the confidence in MWT projections, however, due to the increase detail in fine grid domain models, this paper progresses with the three finer models shown in figure 2.a, 2.c, 2.e.

3.2 Seasonality of MWT; yearly analysis

Due to the range of results from the decadal comparison, fig's 3-9 separately display indices individually. These results focus on the change each year in MWT compared to a global threshold for MOG (98 percentile) turbulence found using all years (and seasons) with the 1950-60 decade. Using a global threshold provides information on the most turbulent projected regions of the globe, most evident through analysis of the y-axis in all subplots in aforementioned figures. In order of most turbulent, Asia, South America, the Antarctic, North America, Africa, Europe and the Australian continent y-axes range from +75 to +275%, 0 to +250%, -50 to 250 %, 0 to +100%, -100 to +60%,-60 to 20% and -95 to -75% respectively. Interestingly, the larger spread highlights differences across the indices and the seasonality of MWT, with winters and summers in both hemispheres characterised with the maxima in MWT in majority of cases. The slopes of the linear regression lines, in figure 3 to 12 (and in section 3.3), are the percentage trend in time per year. However, averaging over an entire continent has lead to a wide spread of results, and in multiple cases has lead to slope errors greater than the absolute slope value. Implying, at a 95% confidence level, that time has no significant linear effect on MWT, with slopes not statistically distinguishable from zero. The percentage of significant trends in each figure is presented in Table 1 and 2, highlighting the variability within the models and lack of confidence in some GCMs. Averages within such tables only include significant slopes.

3.2.1 North America

This paper includes Greenland within North America. However, it should be noted that Greenland has large increases in MWT, evident in figure 2 to 5 and within Section 3.3 where it is discussed further. This may skew an increase in MWT within this sub section, with variability across North America previously shown. Seasonal

https://doi.org/10.5194/egusphere-2025-2378
Preprint. Discussion started: 27 June 2025

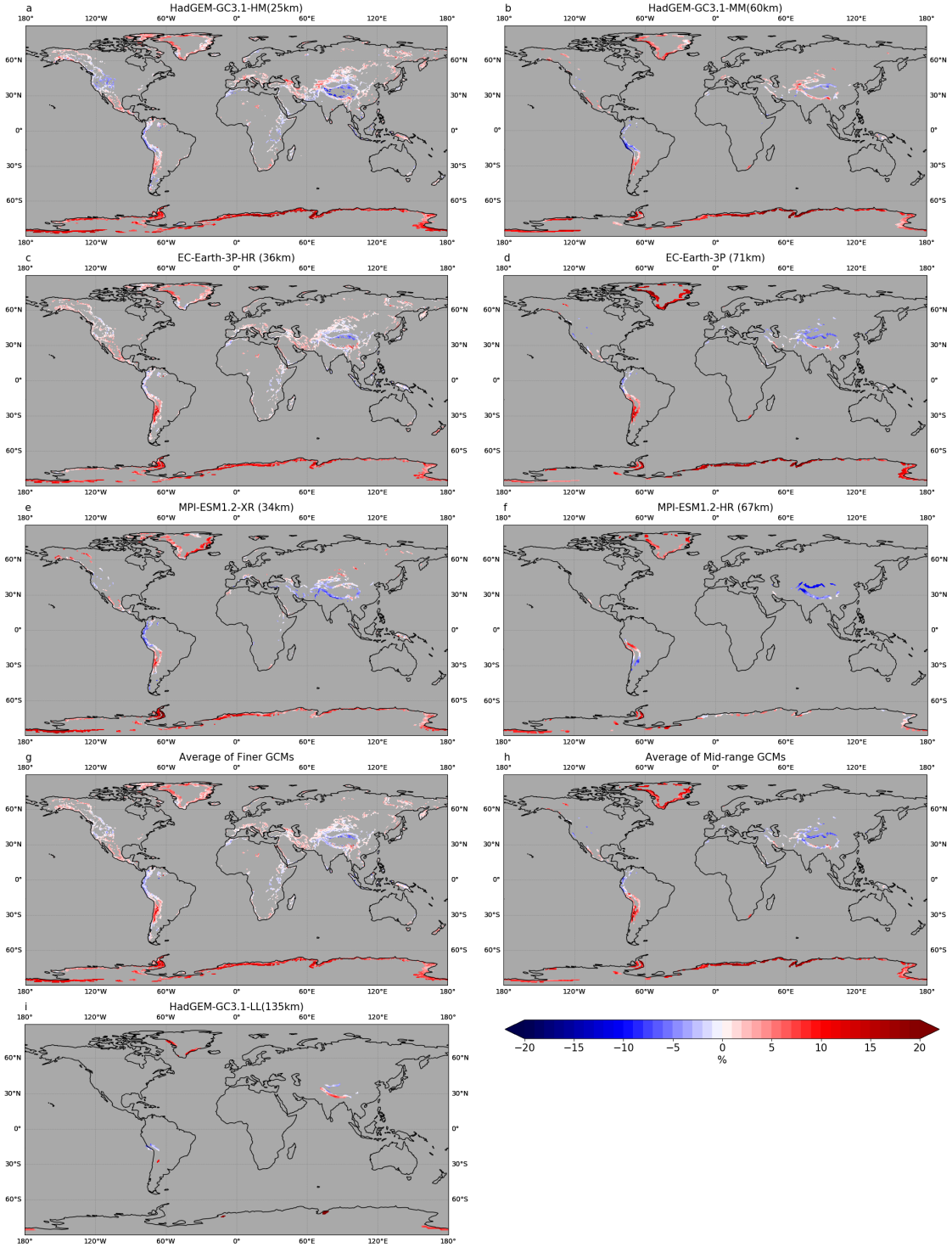

https://doi.org/10.5194/egusphere-2025-2378
Preprint. Discussion started: 27 June 2025

Figure 2. Decade difference in MWT between 1950-59 and 2040-49, for all seven resolutions; HadGEM3-GC3.1-HM 25km,-MM 60km (a,b),-LL 135km (i), EC-Earth-3P-HR 36km,-3P 71km (c,d)and MPI-ESM1.2-XR 34km, HR- 67km (e,f). Subplots g,h show average across finer and mid-range GCMs. Conservative regridding method, modifying data into 36km and 71km across the finer and mid-range domains.

difference in MWT amounts are evident in North America, with percentage changes in winter propagating at higher y-axis values within figure 3's HadGEM3-GC3.1 and EC-Earth-3P subplots. This is expected, with NH winter favourable for MWT generation over USA and Canada, with lowered tropopause heights and peak surface westerlies crossing mountain ranges perpendicularly (Guarino, et al. 2018). Fascinatingly, MPI-ESM1.2 has DJF (December, January, February) and SON (September, October, November) propagate at similar values in MWT_{FD}, MWT_{FDWS}, MWT_{WS} within figure 3, with DJF at times below that of SON and other seasons. A double peak in maxima has been shown in some climatology MWT North America studies. Wolff and Sharman (2008), using PIREP data to find trends in MWT on the United States of America, found peaks in meteorological NH's winter and spring but not necessarily autumn.

A large number of insignificant trends arose across North America, with MWT_{HTG}'s annual, DJF, JJA (June, July, August) results projecting too much variability to definitive show any change in time any of the GCMs. A similar outcome for MWT_{DIV}, with only two slopes projecting a significant trend (EC-Earth-3P annual and HadGEM3-GC3.1-HM SON). Across this continent, only 44 lines, out of 90, project significant trend. Within Table 1, the percentage of slopes, deemed to be significant, within North America are 61.11 %, 33.33 %, 22.22 %, 55.56 % and 72.22% across the entire year, DJF, MAM , JJA and SON respectively. Its evident that the overall annual value is brought up by the higher percentage of confident slopes in SON. Although within Table 1, EC-Earth-3P-HR median in SON is 0.013 +/- 0.034 %/year. This large error occurs due to the range of confident trends, with MWT_{FDWS} and MWT_{HTG} projecting a significant decline but other indices projecting a rise in MWT frequency. Table 1 further displays an overall average increase in MWT over North America, with only these two indices projecting negative slopes in NH autumn. These negatives are highlighted in the range row within Table 1, with SON projecting a change of -4.3 to 16.3% over the 101 year period. Annual, DJF, MAM and JJA return similar ranges within the positive spectrum of 2.4 to 9.5 %, 3.7 to 13.0 %, 3.5 to 8.5% and 2.9% to 10.7%.

NH SON results, on average over the North America continent, have the largest high end positive increase in MWT with the greatest number of significant slopes and the greatest low end projected drop in MWT. On average, SON is projected to increase in MWT by 8.1% from 1950 to 2050. MAM, JJA, DJF and annual on average across this period project a rise by 7.2%, 7.0%, 6.4% and 3.3%, individually.

https://doi.org/10.5194/egusphere-2025-2378
Preprint. Discussion started: 27 June 2025

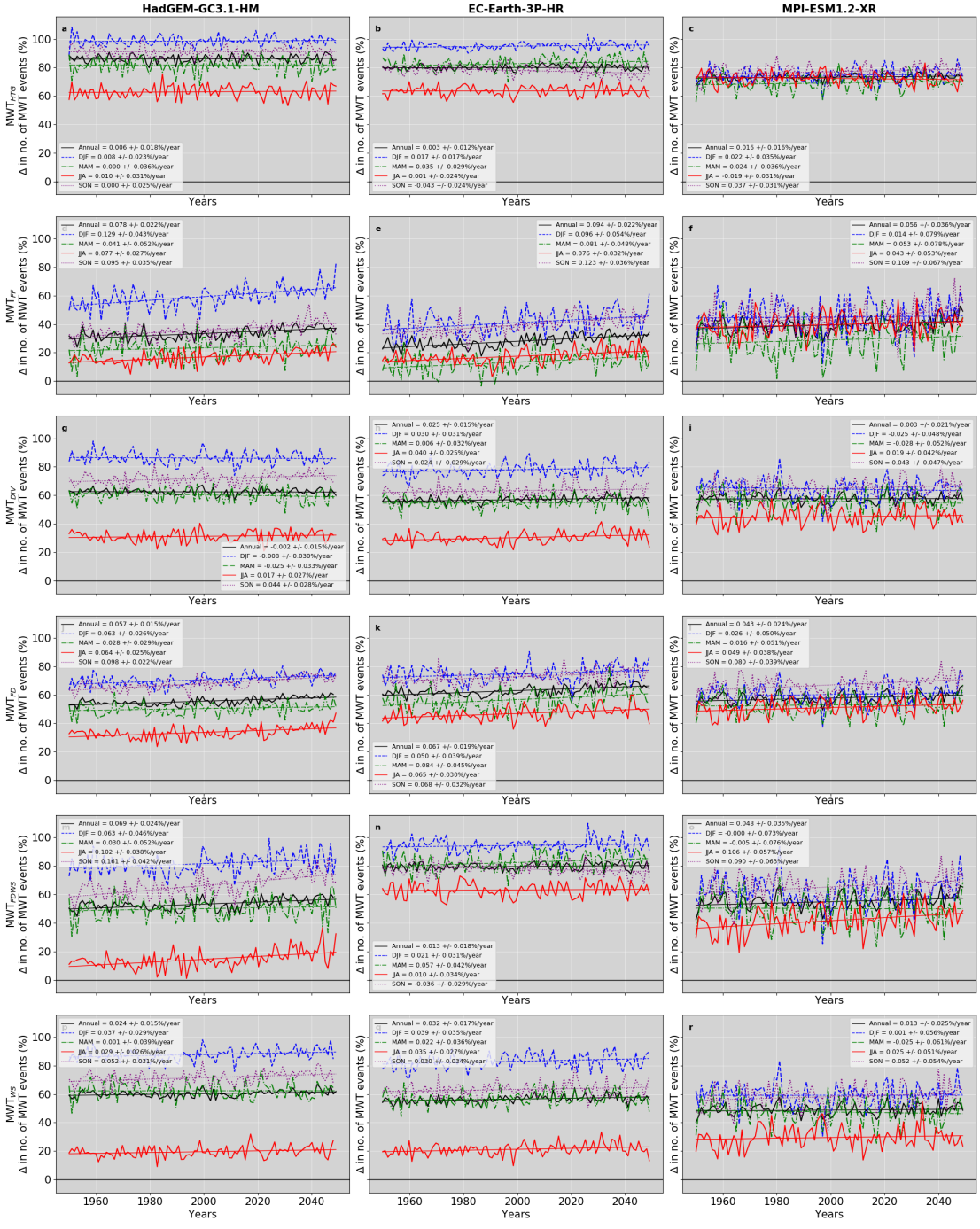

Figure 3. Line plots of relative percentage change over North America for each year and season compared to a 1950 decadal global references, for each GCM; HadGEM3-GC3.1-HM, EC-Earth-3P-HR, and MPI-ESM1.2-XR and for each individual index. Line colour and marking differ for each season, with DJF blue and dashed, MAM green and dash dotted, JJA red and soild, SON purple and dotted. Annual change, which includes all seasons is black and solid.

https://doi.org/10.5194/egusphere-2025-2378
Preprint. Discussion started: 27 June 2025

3.2.2 South America

The annual and seasonal percentage changes in MWT over South America are displayed in figure 4. The y-axis ranging from 0 to 250 %, highlights differences in diagnostics projections, with MWT_{FF} projecting rates that are also found in Asia and the Antarctic (figure 7 & 12). In contracts, EC-Earth-3P-HR's MWT_{FDWS} (figure 4.n) propagates at values are much smaller, similar to rates within Europe and Africa projections (figure 5 & 9). Most other diagnostics propagate around +100%, although there are clear seasonal variations, with SH winter the most turbulent season for all diagnostics, expect MWT_{FF}. In comparison to North America, South America projections have a higher number of significant slopes with 61/90 (67.7%). However, this rate is not evenly spread across the indices. Within figure 4, MWT_{FD} only has five (out of 15) significant trends, with three in MPI-ESM1.2-XR (annual, DJF and JJA) and two in HadGEM3-GC3.1-HM (JJA and SON). Within JJA, MWT_{FDWS}, MWT_{WS} and MWT_{HTG} only have one model each projecting a significant trend. Within Table 1, DJF and annual have a much higher percentage of confident slopes, with 83.3 and 88.9%.

The average over all GCMs across the South America, displayed with Table 1, are interestingly dominated by negatively sloped projections. This suggests a decline in MWT over the period. However, EC-Earth-3P-HR projections often counter this with a rise in MWT frequency. If all three GCMs produced a similar trend (a) and had all indices agreeing, with a high number of significant slopes (b), theoretical weight would be added to the projected outcome. Despite several indices having two or three GCMs meeting condition b), condition a) is met less often in this continent. HadGEM3-GC3.1-HM and MPI-ESM1.2 suggests a decline in MWT in most indices over all seasons and annually in South America. Although there are four positive slopes in the Met. Office Hadley centre model (HadGEM3-GC3.1-HM), for MWT_{FD}'s JJA and SON and MWT_{FF}'s MAM and JJA projections. All indices in the EC-Earth GCM project an increase in MWT apart from MWT_{WS} which displays a decline annually, in DJF and JJA. Section 3.1 determined the largest differences in results between the indices, rather than GCMs. Here a regional dependency is introduced, with South America having larger model disagreement rather than index variation.

3.2.3 Europe

Figure 5's results, which show the change in MWT compared to a global threshold over Europe, propagate below the zero-y-axis line for the majority of the period. This means that this region of the globe has less MWT within the GCMs than the global average. However, DJF values, in many indices, crosses into positive percentage changes, making it a more turbulent season. Interestingly, EC-Earth-3P-HR's MWT_{HTG} and MWT_{FDWS} have spring at a similar propagating level. Almost all MWT_{HTG} lines are significantly sloped, but one in JJA. Overall, this index projects a decline in MWT in all seasons, at most by -0.177%/year in SON, a decrease of 18% over the period. MWT_{DIV}, also projects a decline but DJF or MAM cannot be included in overall analysis with considerable slope error.

https://doi.org/10.5194/egusphere-2025-2378
Preprint. Discussion started: 27 June 2025

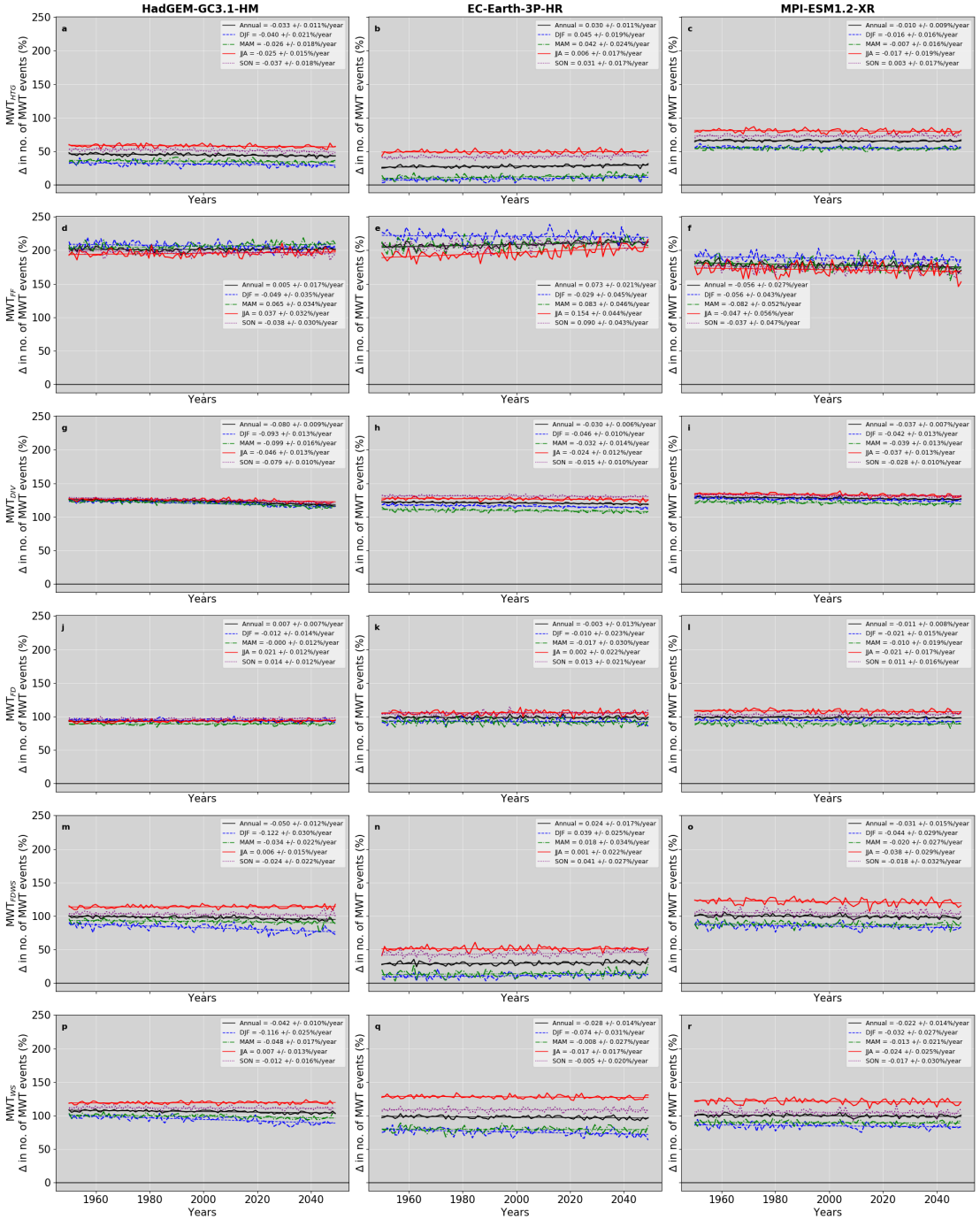

Figure 4. Line plots of relative percentage change over South America for each year and season compared to a 1950 decadal global references, for each GCM; HadGEM3-GC3.1-HM, EC-Earth-3P-HR, and MPI-ESM1.2-XR and for each individual index. Line colour and marking differ for each season, with DJF blue and dashed, MAM green and dash dotted, JJA red and soild, SON purple and dotted. Annual change, which includes all seasons is black and solid.

https://doi.org/10.5194/egusphere-2025-2378
Preprint. Discussion started: 27 June 2025

However, MWT_{FF}, MWT_{FD} and MWT_{WS} all project an increase in their significant slopes. The remaining index, MWT_{FDWS}, has opposing signs across GCMs with HadGEM3-GC3.1 suggesting an increase with the previous three indices and EC-Earth-3P-HR projecting a reduction in MWT. MPI-ESM1.2 has no significant slopes within this index. As evident from Table 1, when averaging across this figure, DJF, MAM and annual project an increase of 0.043, 0.057 and 0.039 %/year. An almost opposite response apparent in SON, with -0.045 % per year. JJA has too much variability to show any clear response. Like South America, Europe did not meet condition a) but it also did not meet condition b), with large variations across both models and indices, suggesting a less confident response.

3.2.4 Africa

Figure 6 displays the percentage change in MWT over the African continent. The most notable result within this figure is the level on the y-axis that HadGEM3-GC3.1's MWT_{FF} lines propagate at. This height on the y-axis is comparable with the amount of turbulence over North America. This index previously projected relatively large percentage changes, compared to the other five indices, in section 3.2.2 over South America. Most indices in Africa reside in the negative spectrum, with the amount of MWT turbulence similar to Europe or below. One index of interest, when considering the trend of the data, is MWT_{DIV}. All three GCMs agree, all with significant slopes, that MWT, diagnosed by MWT_{DIV}, is decreasing over Africa in all seasons. The remaining 5 indices do not have all three GCMs producing significant slopes or have them agreeing on a trend. There are multiple indices that do agree with the decline in JJA, SON, DJF and annually, as seen by the overall average decrease in such seasons in Table 1. However, MAM has a wide range of significant slopes, and overall ends up projecting a positive trend of 1% over the 101 years.

3.2.5 Asia

Due to the Himalayan Mountains and many other steep mountain ranges over Asia, the MWT percentages on the y-axis in figure 7 are the largest compared to any other continent. The seasonality of MWT is very interesting over Asia, with different indices projecting MAM, JJA or DJF to have the maxima in MWT across their retrospective subplots. In section 3.3, regional analysis should help further understanding on the mix of seasonal maximums. Interestingly, MWT_{FF} again projects the largest percentage change ranges within figure 7 . In this case many other indices are propagating at a percentage value near or just below this index, adding confidence in the high amount of MWT over Asia.

As shown by slopes in figure 7 and Table 2, there is a mix in projected trends for MAM and SON. Within MAM results, MWT_{HTG} and MWT_{DIV} generally projecting a decrease, and MWT_{FF}, MWT_{FD}, MWT_{FDWS} and MWT_{WS} suggesting an increase. MWT_{FF} large slopes of +0.126, +0.193 and +0.072 shift the tug of war between the indices and suggest an overall increase in MAM. In SON, despite MWT_{FF} producing slopes of +0.23, +0.25 and +0.11%/year, MWT_{DIV} negative tilts of -0.143,0.123 and -0.043%/year, combined with negative results from

https://doi.org/10.5194/egusphere-2025-2378
Preprint. Discussion started: 27 June 2025

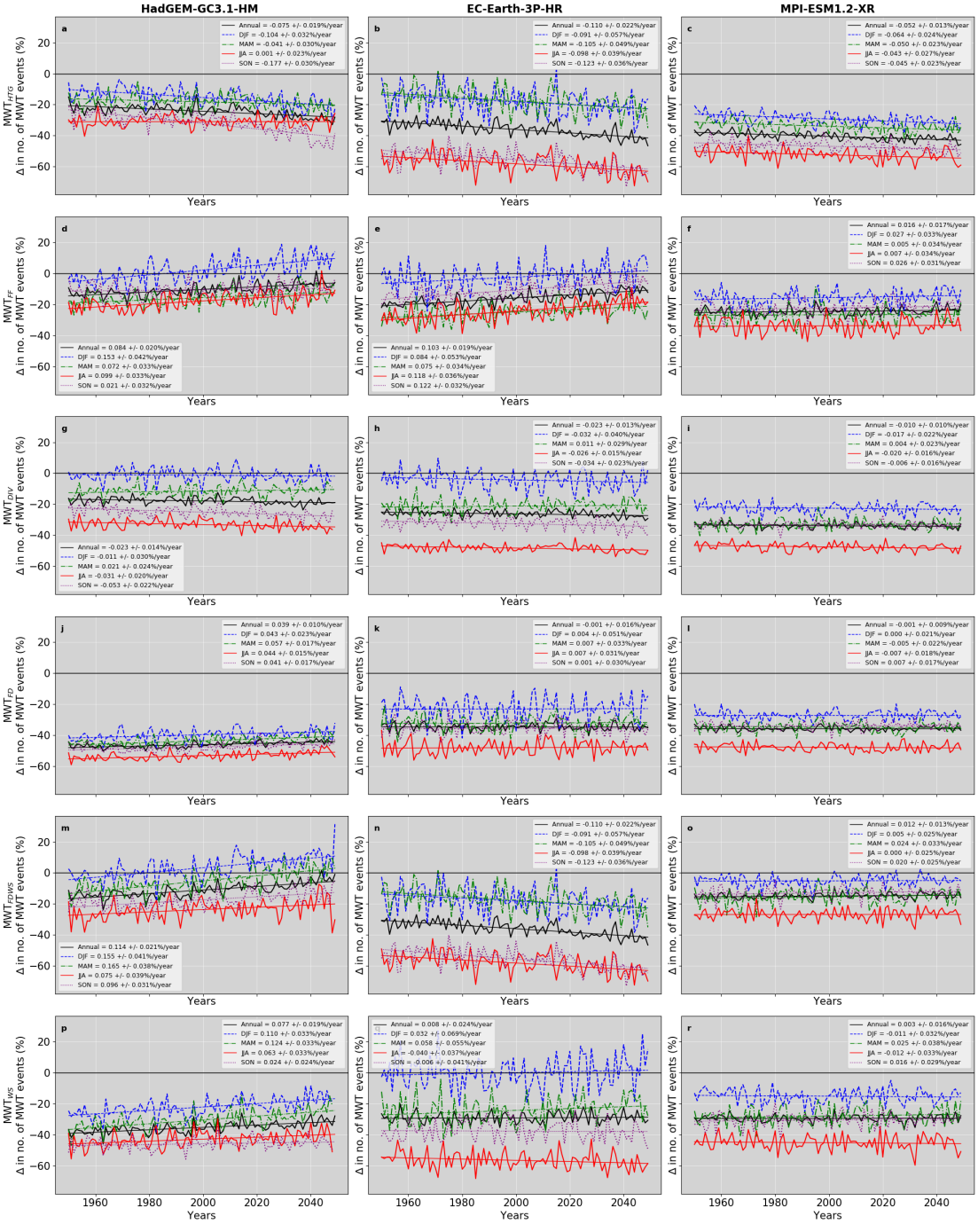

Figure 5. Line plots of relative percentage change over Europe for each year and season compared to a 1950 decadal global references, for each GCM; HadGEM3-GC3.1-HM, EC-Earth-3P-HR, and MPI-ESM1.2-XR and for each index. Line colour and marking differ for each season, with DJF blue and dashed, MAM green and dash dotted, JJA red and soild, SON purple and dotted. Annual change, which includes all seasons is black and solid.

https://doi.org/10.5194/egusphere-2025-2378
Preprint. Discussion started: 27 June 2025

other indices, produces a median within Table 2 of -0.055 %/year. Within DJF and JJA, most slopes project an increase and a decrease in MWT, respectively. Over the 101-year period, DJF over Asia is projected to increase on average by +7 %, and at maximum by +30.9 % (MWT_{FF}, HadGEM3-GC3.1-HM). Interestingly, only 50% of DJF and JJA lines within figure 7, have significant trends. A larger percentage is evident in MAM and SON.

3.2.6 Australian Continent

A strong seasonal gap arose in the slopes over the Australian continent within figure 8, with a clear decrease in MWT over DJF and MAM (summer and autumn) and an evident increase for JJA and SON (winter and spring). The conditions of a) having all GCMs and b) all indices agreeing has been mostly met by this continent. JJA has all GCMs and indices producing significant trends, all projecting an increase. As displayed within Table 2, the average increase is of around +1.4 % with a maximum +4.4 % and minimum of +0.6 % over the 101 year period. SON also had a very similar agreement and trend but a lower number of significant slopes, at 72.22 % across figure 8. In terms of amount of turbulence, compared to the other six continents, the y-axis is at its most negative on average, with a much smaller range. In terms of which season is on general most turbulent, in regards to MWT, JJA, SON and DJF are all at one point projected to have the largest amount of turbulence in at least one GCM and index.

3.2.7 Antarctic

There is a clear seasonality in the amount of MWT over the Antarctic, with SH winter and summer being the most and least turbulent season. The large JJA (winter) values in figure 9 place this continent second, after Asia, with the amount of projected MWT with the GCMs. Within this figure, only 6 projections suggest a decline in MWT within this region. There are 3 lines in JJA and 3 lines in SON across MWT_{HTG} and MWT_{FDWS} projections that show this decrease in MWT over the period. Despite this, there is quite strong model and index agreement, with all other indices, across all GCMs, projecting a significant increase in MWT. DJF on average projected a rise of +32% compared to the amount in 1950. JJA, the most turbulent season, had an increase of +8.7%. Few airlines travel over the Antarctic, but this result does put those few airlines at risk travelling, particularly in SH summer.

3.3 Regional analysis

Section 3.1 highlighted sub-continental differences across the globe. Figure 10, 11 and 12 focus on twenty-eight new smaller sub-continental areas of interest. Within these figures, results come from an average across indices with a significant trend. In some cases all six indices within the GCM are projecting insignificant trends so the model is not considered or plotted. This is noticeable by the lack of scatter from some GCMs in figure 10 side plots and grey shaded blocks within figure 11. Similar to figure 2g, the spatial map in figure 10 is the 1950-59 to 2040-49 decade percentage difference averaged over the three finest GCMs, regridded on to the EC-Earth domain. However, if an index is not included in the scatter plots (insignificant) it has therefore been removed from each sub region in the

https://doi.org/10.5194/egusphere-2025-2378
Preprint. Discussion started: 27 June 2025

		North America	South America	Europe	Africa
Yearly	Slope Median	0.033 +/- 0.019	-0.015 +/- 0.010	0.039 +/- 0.020	-0.012 +/- 0.005
	Had Median	0.063 +/- 0.018	-0.042 +/- 0.010	0.058 +/- 0.019	-0.013 +/- 0.004
	EC Median	0.050 +/- 0.018	0.024 +/- 0.014	-0.066 +/- 0.021	-0.015 +/- 0.005
	MPI Median	0.028 +/- 0.021	-0.014 +/- 0.008	0.045 +/- 0.029	-0.012 +/- 0.006
	Range	0.024 +/- 0.015	-0.080 +/- 0.009	-0.110 +/- 0.022	-0.064 +/- 0.004
		to 0.094 +/- 0.022	to 0.073 +/- 0.021	to 0.114 +/- 0.021	to 0.017 +/- 0.007
	Sig (%)	61.11	88.89	72.22	55.56
	no.pos , no. neg	11 , 0	4, 12	8, 5	1, 9
DJF	Slope Median	0.063 +/- 0.041	-0.044 +/- 0.025	0.043 +/- 0.041	-0.032 +/- 0.009
	Had Median	0.063 +/- 0.036	-0.093 +/- 0.025	0.110 +/- 0.033	-0.036 +/- 0.011
	EC Median	0.073 +/- 0.046	-0.002 +/- 0.024	-0.091 +/- 0.057	-0.032 +/- 0.010
	MPI Median	NA	-0.037 +/- 0.021	-0.064 +/- 0.024	-0.008 +/- 0.004
	Range	0.037 +/- 0.029	-0.122 +/- 0.030	-0.104 +/- 0.032	-0.057 +/- 0.007
		to 0.129 +/- 0.043	to 0.045 +/- 0.019	to 0.155 +/- 0.041	to -0.008 +/- 0.004
	Sig (%)	33.33	83.33	50.00	33.33
	no.pos, no. neg	6, 0	2, 13	5, 4	0, 6
MAM	Slope Median	0.071 +/- 0.047	-0.033 +/- 0.020	0.057 +/- 0.034	0.010 +/- 0.007
	Had Median	NA	-0.034 +/- 0.018	0.072 +/- 0.033	0.024 +/- 0.015
	EC Median	0.071 +/- 0.047	0.042 +/- 0.024	-0.024 +/- 0.049	0.010 +/- 0.007
	MPI Median	NA	-0.060 +/- 0.032	-0.050 +/- 0.023	-0.009 +/- 0.004
	Range	0.035 +/- 0.029	-0.099 +/- 0.016	-0.105 +/- 0.049	-0.059 +/- 0.007
		to 0.084 +/- 0.047	to 0.083 +/- 0.046	to 0.165 +/- 0.038	to 0.033 +/- 0.019
	Sig (%)	22.22	55.56	55.56	55.56
	no.pos, no. neg	4, 0	3, 7	6, 4	6, 4
JJA	Slope Median	0.069 +/- 0.032	-0.023 +/- 0.016	-0.023 +/- 0.033	-0.012 +/- 0.007
	Had Median	0.070 +/- 0.026	-0.002 +/- 0.014	0.063 +/- 0.033	-0.025 +/- 0.011
	EC Median	0.057 +/- 0.032	-0.019 +/- 0.018	-0.040 +/- 0.037	-0.008 +/- 0.007
	MPI Median	0.077 +/- 0.047	-0.037 +/- 0.017	-0.032 +/- 0.021	-0.009 +/- 0.006
	Range	0.029 +/- 0.026	-0.046 +/- 0.013	-0.098 +/- 0.039	-0.052 +/- 0.011
		to 0.106 +/- 0.057	to 0.154 +/- 0.044	to 0.118 +/- 0.036	t o 0.024 +/- 0.016
	Sig (%)	55.56	55.56	66.67	55.56
	no.pos, no. neg	10, 0	3, 7	5, 7	1, 9
SON	Slope Median	0.080 +/- 0.035	-0.019 +/- 0.018	-0.045 +/- 0.030	-0.016 +/- 0.008
	Had Median	0.095 +/- 0.031	-0.037 +/- 0.018	-0.006 +/- 0.026	-0.034 +/- 0.008
	EC Median	0.013 +/- 0.034	0.036 +/- 0.024	-0.078 +/- 0.034	-0.015 +/- 0.009
	MPI Median	0.085 +/- 0.051	-0.028 +/- 0.010	-0.045 +/- 0.023	-0.014 +/- 0.007
	Range	-0.043 +/- 0.033	-0.079 +/- 0.010	-0.177 +/- 0.030	-0.091 +/- 0.008
		to 0.161 +/- 0.042	to 0.090 +/- 0.043	to 0.122 +/- 0.032	to 0.028 +/- 0.012
	Sig (%)	72.22	55.56	50.00	55.56
	no.pos, no. neg	11, 2	4, 6	3, 6	1, 9

Table 1. Seasonal and annual median slope values from figure 3 to 6 across each GCM with HadGEM3-GC3.1-HM referenced as "Had", EC-Earth-3P-HR as "EC" and MPI-ESM1.2-XR as "MPI". "Range" displays the spread across all significant slopes over GCMs. "Sig" displays the percentage of slopes for each season with significant slopes. "no. pos, no. neg" values indicating the number of significant positive or negative slopes.

https://doi.org/10.5194/egusphere-2025-2378
Preprint. Discussion started: 27 June 2025

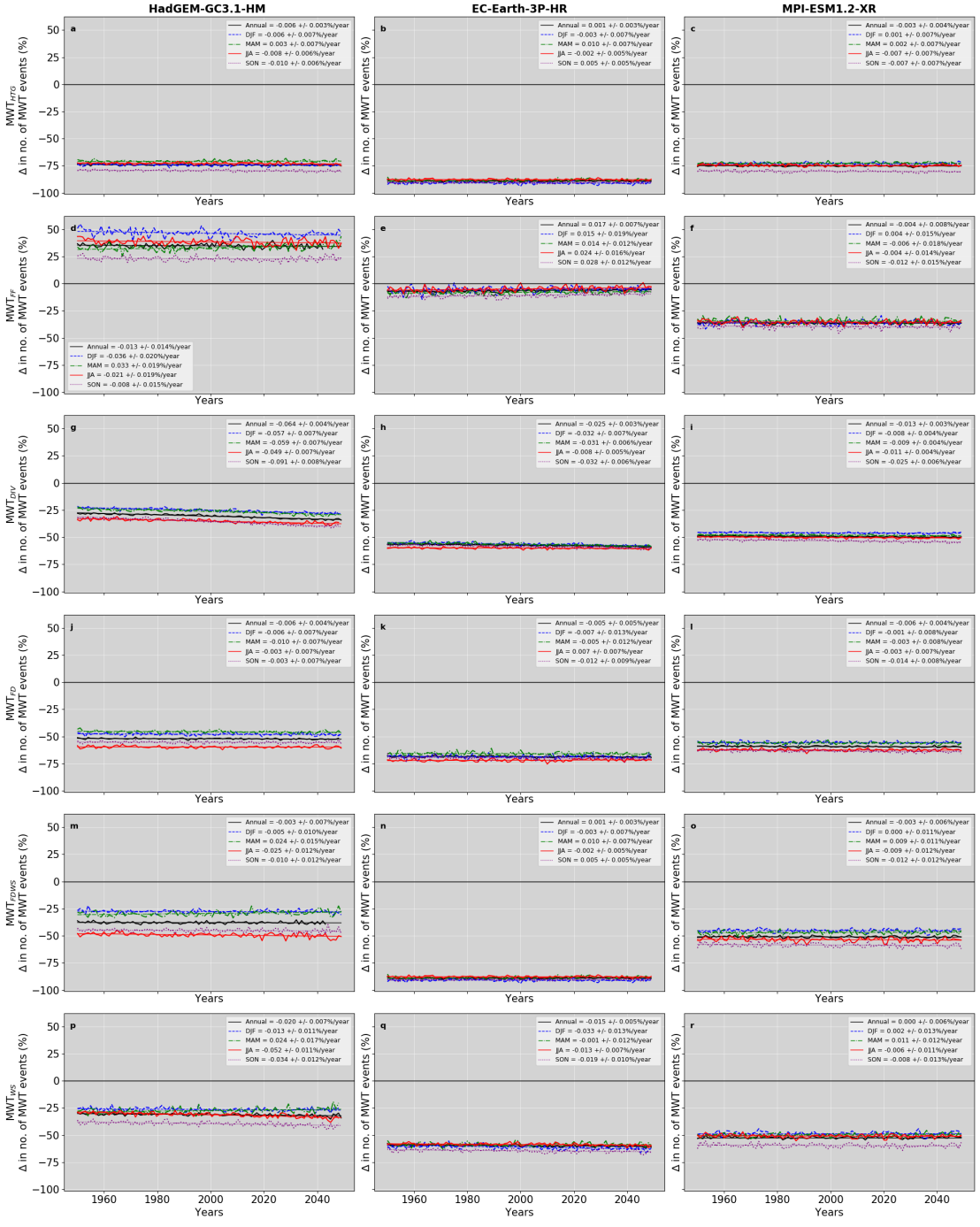

Figure 6. Line plots of relative percentage change over Africa for each year and individual season compared to a 1950 decadal global references, for each GCM; HadGEM3-GC3.1-HM, EC-Earth-3P-HR, and MPI-ESM1.2-XR and for each index. Line colour and marking differ for each season, with DJF blue and dashed, MAM green and dash dotted, JJA red and soild, SON purple and dotted. Annual change, which includes all seasons is black and solid.

https://doi.org/10.5194/egusphere-2025-2378
Preprint. Discussion started: 27 June 2025

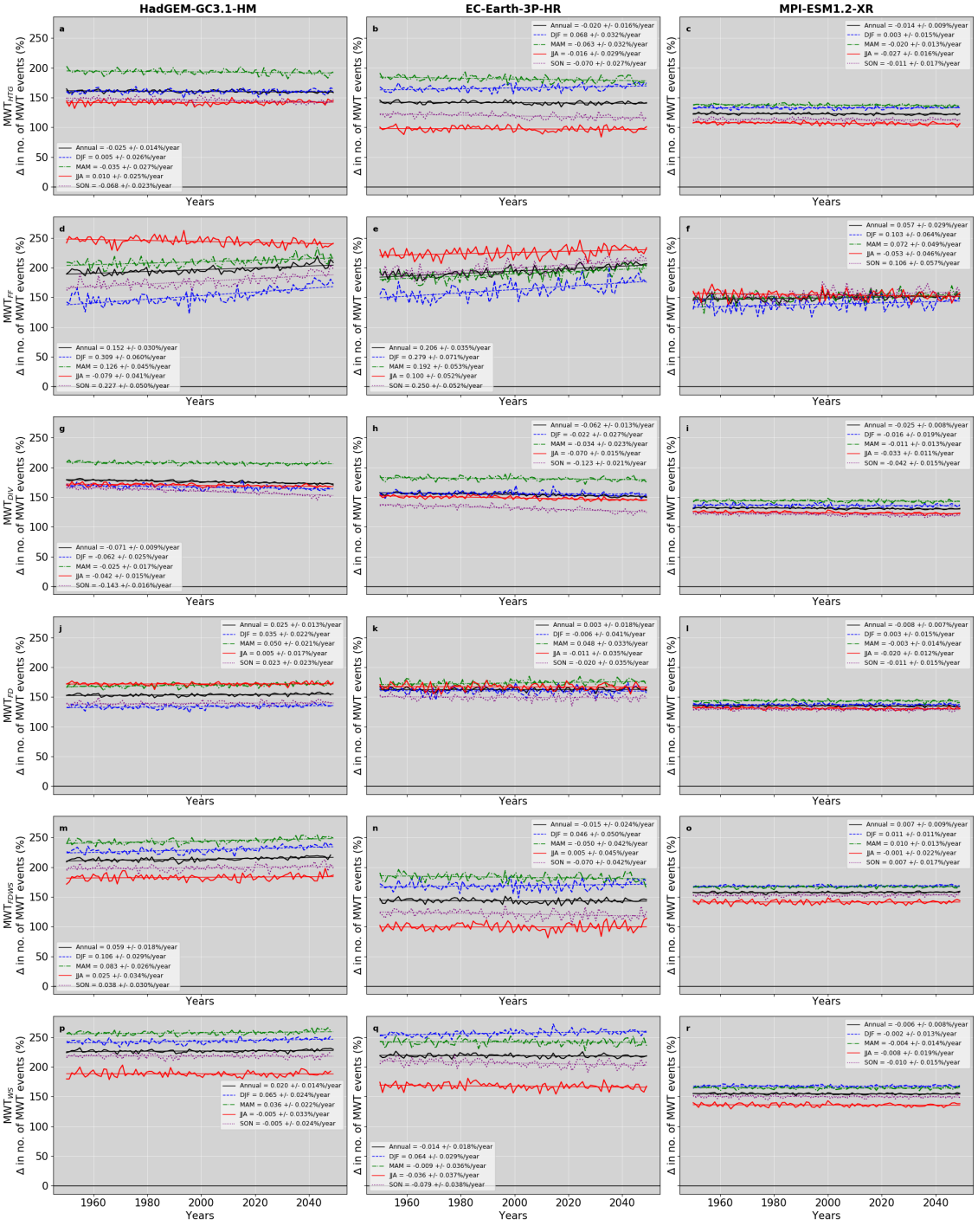

Figure 7. Line plots of relative percentage change over the Asian continent for each year and season compared to a 1950 decadal global references, for each GCM; HadGEM3-GC3.1-HM, EC-Earth-3P-HR, and MPI-ESM1.2-XR and for each individual index. Line colour and marking differ for each season, with DJF blue and dashed, MAM green and dash dotted, JJA red and soild, SON purple and dotted. Annual change, which includes all seasons is black and solid.

https://doi.org/10.5194/egusphere-2025-2378
Preprint. Discussion started: 27 June 2025

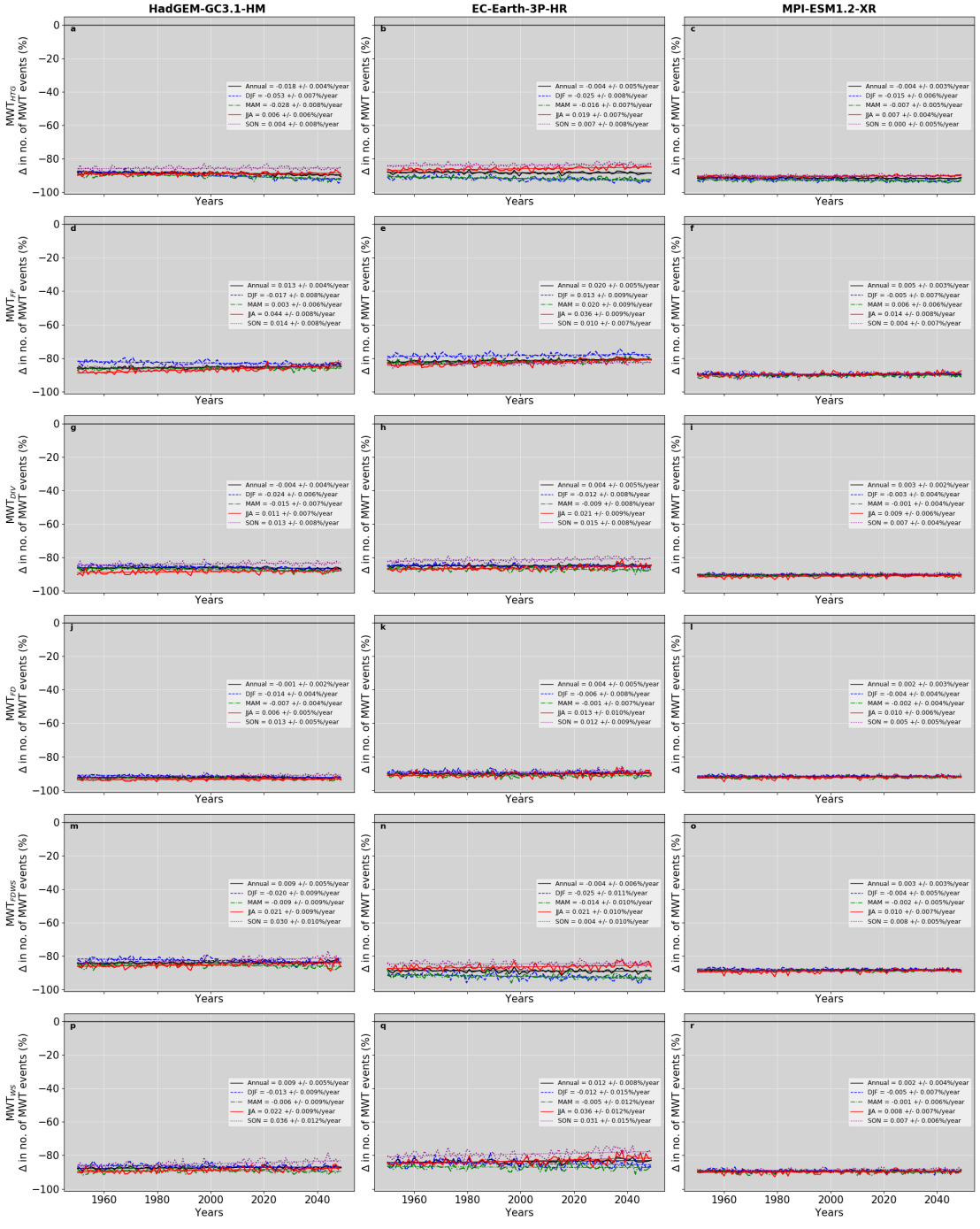

Figure 8. Line plots of relative percentage change over the Australian continent for each year and season compared to a 1950 decadal global references, for each GCM; HadGEM3-GC3.1-HM, EC-Earth-3P-HR, and MPI-ESM1.2-XR and for each individual index. Line colour and marking differ for each season, with DJF blue and dashed, MAM green and dash dotted, JJA red and solid, SON purple and dotted. Annual change, which includes all seasons is black and solid.

https://doi.org/10.5194/egusphere-2025-2378
Preprint. Discussion started: 27 June 2025

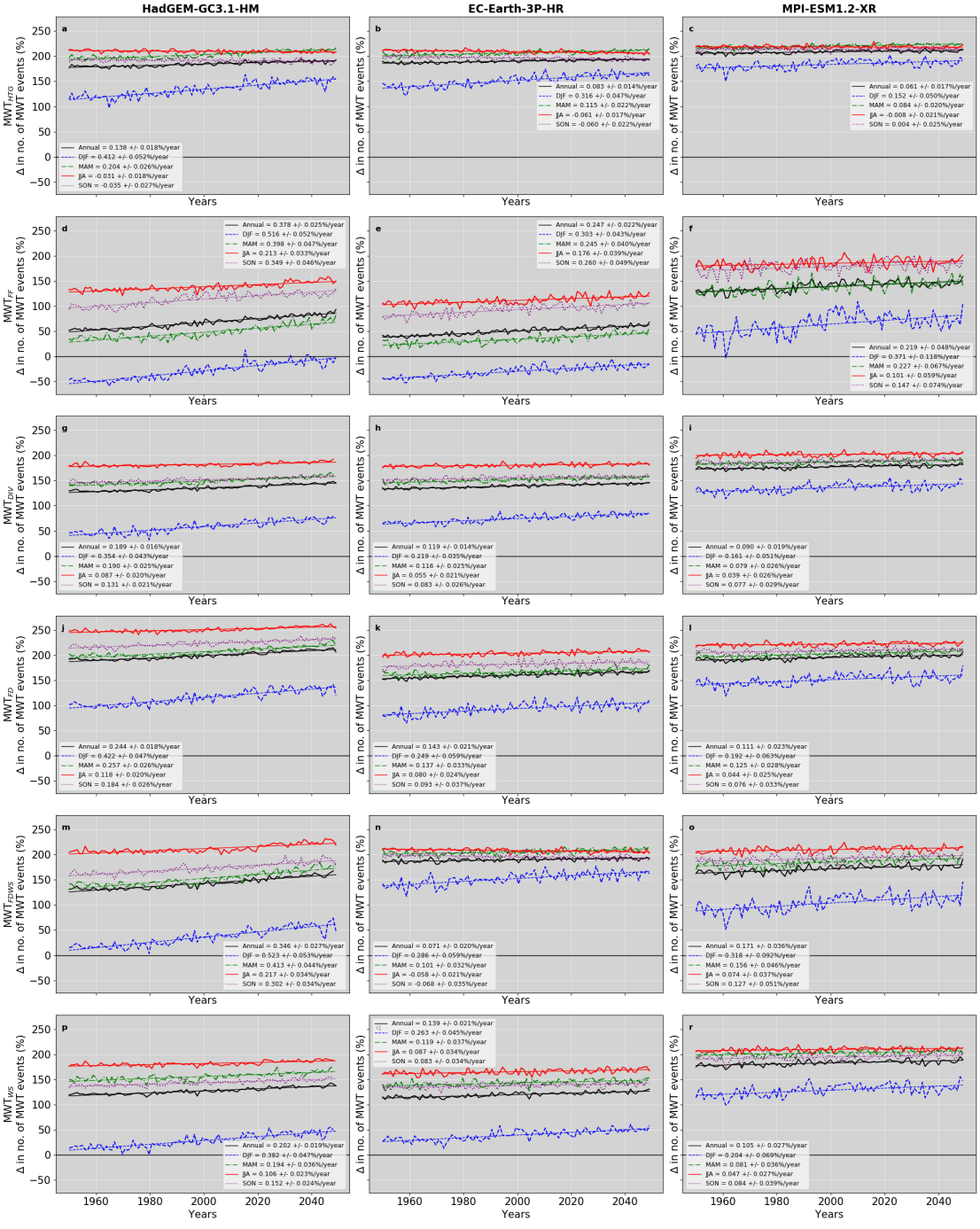

Figure 9. Line plots of relative percentage change over the Antarctic for each year and season compared to a 1950 decadal global references, for each GCM; HadGEM3-GC3.1-HM, EC-Earth-3P-HR, and MPI-ESM1.2-XR and for each individual index. Line colour and marking differ for each season, with DJF blue and dashed, MAM green and dash dotted, JJA red and soild, SON purple and dotted. Annual change, which includes all seasons is black and solid.

https://doi.org/10.5194/egusphere-2025-2378
Preprint. Discussion started: 27 June 2025

		Asia	Australia	Antarctic
Yearly	Slope Median	0.024 +/- 0.016	0.007 +/- 0.004	0.129 +/- 0.019
	Had Median	0.022 +/- 0.014	0.009 +/- 0.005	0.223 +/- 0.019
	EC Median	-0.020 +/- 0.016	0.016 +/- 0.006	0.129 +/- 0.021
	MPI Median	0.025 +/- 0.016	-0.002 +/- 0.002	0.084 +/- 0.019
	Range	-0.071 +/- 0.009	-0.018 +/- 0.004	0.046 +/- 0.014
		to 0.206 +/- 0.035	to 0.020 +/- 0.005	to 0.378 +/- 0.025
	Sig (%)	77.78	55.56	100.00
	no.pos, no. neg	9, 5	6, 4	18, 0
DJF	Slope Median	0.070 +/- 0.029	-0.018 +/- 0.008	0.317 +/- 0.051
	Had Median	0.065 +/- 0.025	-0.019 +/- 0.007	0.417 +/- 0.050
	EC Median	0.070 +/- 0.032	-0.018 +/- 0.009	0.289 +/- 0.046
	MPI Median	0.103 +/- 0.064	-0.015 +/- 0.006	0.198 +/- 0.066
	Range	-0.062 +/- 0.025	-0.053 +/- 0.007	0.152 +/- 0.050
		to 0.309 +/- 0.060	to 0.013 +/- 0.009	0.523 +/- 0.053
	Sig (%)	50.00	66.67	100.00
	no.pos, no. neg	8, 1	1, 11	18, 0
MAM	Slope Median	0.036 +/- 0.027	-0.009 +/- 0.008	0.149 +/- 0.032
	Had Median	0.043 +/- 0.024	-0.012 +/- 0.008	0.231 +/- 0.031
	EC Median	-0.034 +/- 0.032	-0.012 +/- 0.00	0.123 +/- 0.032
	MPI Median	0.026 +/- 0.031	-0.007 +/- 0.005	0.104 +/- 0.032
	Range	-0.063 +/- 0.032	-0.028 +/- 0.008	0.079 +/- 0.026
		to 0.192 +/- 0.053	to 0.020 +/- 0.009	to 0.413 +/- 0.044
	Sig (%)	72.22	50.00	100.00
	no.pos, no. neg	7, 6	1, 8	18, 0
JJA	Slope Median	-0.042 +/- 0.016	0.014 +/- 0.008	0.087 +/- 0.026
	Had Median	-0.061 +/- 0.028	0.016 +/- 0.008	0.112 +/- 0.022
	EC Median	-0.042 +/- 0.041	0.022 +/- 0.010	0.071 +/- 0.025
	MPI Median	-0.030 +/- 0.014	0.009 +/- 0.006	0.047 +/- 0.027
	Range	-0.079 +/- 0.041	0.006 +/- 0.005	-0.064 +/- 0.023
		to 0.100 +/- 0.052	to 0.044 +/- 0.008	to 0.217 +/- 0.034
	Sig (%)	50.00	100.00	94.44
	no.pos, no. neg	1, 8	18, 0	14, 3
SON	Slope Median	-0.055 +/- 0.029	0.013 +/- 0.008	0.104 +/- 0.034
	Had Median	0.023 +/- 0.023	0.014 +/- 0.008	0.168 +/- 0.026
	EC Median	-0.074 +/- 0.042	0.014 +/- 0.009	0.087 +/- 0.039
	MPI Median	0.032 +/- 0.036	0.007 +/- 0.005	0.084 +/- 0.039
	Range	-0.143 +/- 0.016	0.0049 +/- 0.0046	-0.074 +/- 0.040
		to 0.250 +/- 0.052	to 0.036 +/- 0.012	to 0.349 +/- 0.046
	Sig (%)	66.67	72.22	94.44
	no.pos, no. neg	5, 7	13, 0	14, 3

Table 2. Seasonal and annual median slope values from figure 7 to 9 across each GCM with HadGEM3-GC3.1-HM referenced as "Had", EC-Earth-3P-HR as "EC" and MPI-ESM1.2-XR as "MPI". The same rows as Table 2, but with three final continents.

https://doi.org/10.5194/egusphere-2025-2378
Preprint. Discussion started: 27 June 2025

spatial map, which averages across all GCMs and indices. However, when processing these figures, one should take care to note the spatial map in figure 10, which shows the decadal difference averaged across all seasons. If you break down the percentage change scatter in to each season (figure 11), differences in seasonal trends arise. Figure 11 breaks down the seasonal change for each region, averaged across the six MWT diagnostics.

The trends over a 101 year period are discussed below. Further analysis was done, focusing on a future 30 year period (2020-2050) but is not included within this section due to large decadal variability within findings. Interestingly in some cases significance shifted, with some trends previously showing a trend no longer applicable and vice versa. This shows that having an 101 year period more effectively encapsulates the MWT trends in time, with a 30 year periods linked to decadal variability.

3.3.1 North America; NA1-NA5

The North American continent is broken down into five regional areas. Region NA1 covers Greenland, Iceland and Canada north to north east of the Hudson bay. Aircraft are known to travel through this region, particularly over southern Greenland, when flying from Europe to North America and vice versa (Lane,2009). MWT formation over Greenland is often associated with the passage of a surface cyclone, due to progression of easterly or south easterly wind flow over the mountains terrain, with 40% of all significant turbulent events linked with this type of generation (Lane et al., 2009). As discussed in Section 3.2, the percentage change is compared to a global average value of MOG MWT (dependent on index and model) and therefore percentage change on the y-axis of figure 10's scatter plots represents the amount of MWT in each region. NA1 is the second most turbulent region in North America. Greenland is a known turbulent region of the globe, with every fourth day having at least one MOG turbulent PIREP report (Lane et al, 2009). In terms of seasonality, literature suggest MWT frequency is similar to contiguous United States (CONUS), where some winter months (January) have had rates four times the amount of MOG MWT compared to spring months (May) (Lane et al,2009, Wolff and Sharman 2008).

Interestingly, NH summer HadGEM3-GC3.1-HM projections had the greatest average increase of +58.4 % over the 101 year period within NA1 (figure 11). Once averaged over all GCMs that's an increase of +30.5 % between 1950 to 2050 for the summer season (JJA). NH autumn and spring project the same trend but at lower rates of +19.4 % and +18.0 % respectively. Interestingly, winter changes are more difficult to diagnose, with all indices projecting high inter-annual variability and insignificant trends , and therefore not included in figure 11 . Therefore, no definitive trends in MWT over NA1 in DJF. However, there are trends within surface winds speeds for NH winter between 1950 to 2050, evident in figure 12. Within this season, SON and MAM, an increase in median surface winds were projected, but weaker maximum wind speed. The evident increase in MWT frequency in SON and MAM could be linked to the average wind speeds, with increase evident in figure 12. However, the projected increase in MWT in JJA's, previously touched, within NA1 is not correlated to the surface wind speed changes, with a slight decline

https://doi.org/10.5194/egusphere-2025-2378
Preprint. Discussion started: 27 June 2025

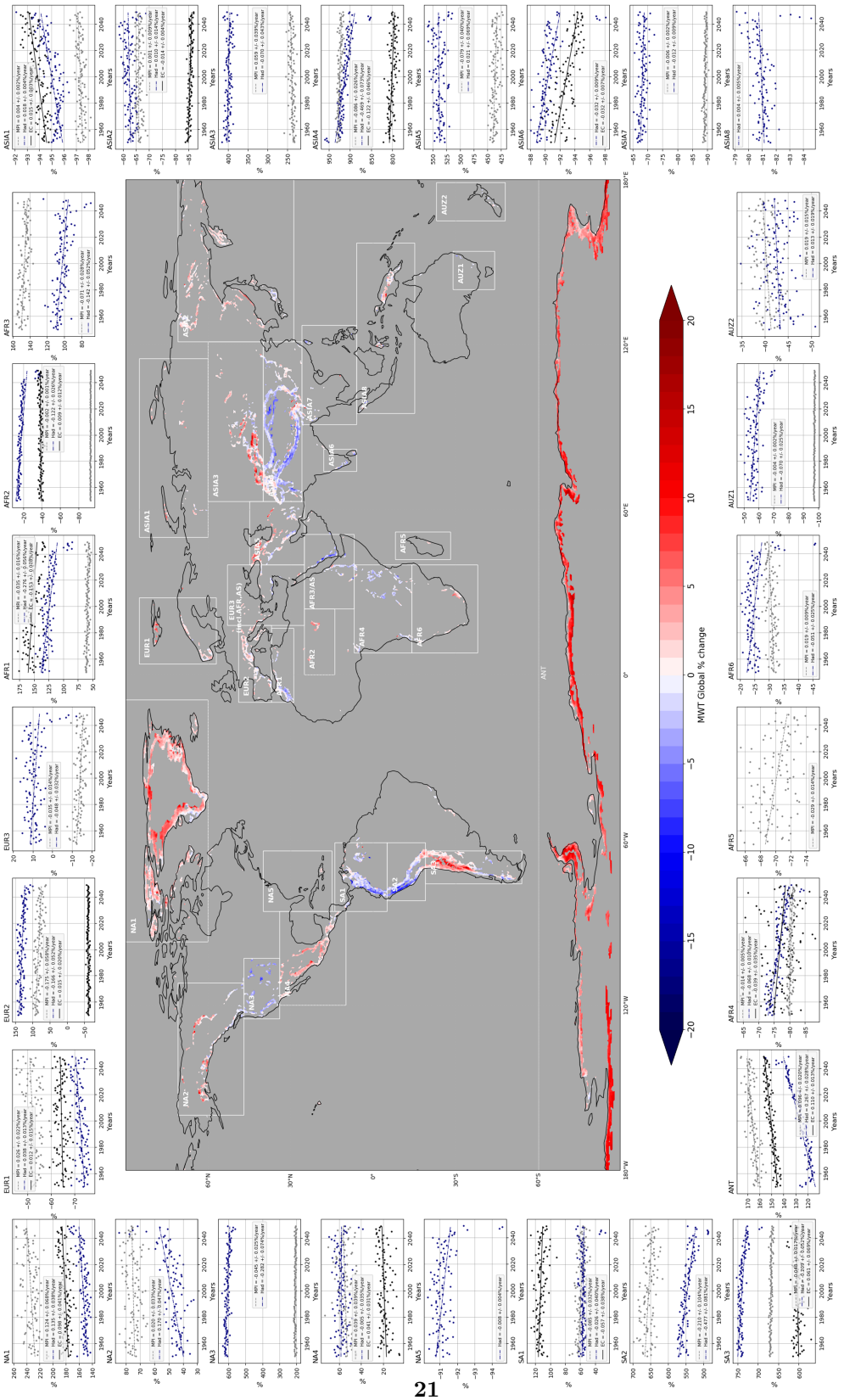

https://doi.org/10.5194/egusphere-2025-2378
Preprint. Discussion started: 27 June 2025

Figure 10. The spatial map displays the percentage difference between the 1950s and 2040s averaged across the three finer GCMs, similar to figure 5.2(g), but for each 28 regions. If indices are insignificant over a 101-year period, they are not included within area averaging. The line plots surrounding the map show the relative MWT percentage change from global threshold for each year, averaged over six MWT indices, for each new sub-region shown by a white box. HadGEM3-GC3.1-HM linear regression slopes and scatter are referred to as "Had", as previously done in Table 5.1 and 2, and coloured navy with a dash-dot line. MPI-ESM1.2-XR is referred to as "MPI" with a grey scatter and dashed linear regression line. EC-Earth-3P-HR is referred to as "EC" with black scatter and a solid line.

in median surface wind change for the HadGEM3-GC3.1-HM model. Only trends with significant slopes have been shown within figure 12, as done in the previous last two figures.

Within figure 10, regions NA2 and NA4 are clearly projected to increase over the 101 year period. Here one can also note projected insignificant sloped lines in the side scatter plots. Despite all indices projecting a confident trend, their trends range in both the negative and positive spectrum. This has led to an overall average uncertainty within the scatter. EC-Earth-3P-HR's indices did not produce significant trends to be included initially in NA2 region, but within a break down of seasonality, its clearly linked to the model projecting a drop in MWT in NH summer and increase in NH autumn. NA4 projections too have a seasonal difference, with a general increase in all seasons but SON. Over all GCMs NH winter, summer, spring and autumn MWT rates are projected to shift by +21.6 % , -1.4% , +12.4 % and +17.9 % within NA2 over 101 years and by +7.2 % , +1.6 % -10.5 % and +10.9 % within NA4, respectively. In terms of relationships to surface wind speed, within NA2, DJF and JJA median surface wind speed projections corolate to the same positive or negative shift found in MWT results. This is not the case for SON and MAM, with opposing trends. A similar outcome arose for NA4 in terms of the relationship between low-level wind speed shift and the change in seasonal MWT frequency.

NA3 encapsulates part of the Rocky Mountain range, and is the projected most turbulent (mountain generated) region of North America, with HadGEM3-GC3.1-HR data scattered at the 600% range. The Rocky Mountains are a well documented turbulent area (Wilms, Henrike 2020), with MWT the major source of turbulence over the western half of the USA (Wolff and Sharman,2008). Figure 10 and 14 show a decline for MWT over NA3 for all seasons but DJF (NH winter). EC-Earth-3P-HR DJF projections, averaged across significant indices, suggest an incredible slope of +1.64 %/year within this season. This steep slope is damped once averaged across GCMs, but overall they suggest an increase of 60.6% over the 101 years. NH summer, autumn and spring project a decrease of -58.3%, -30.9% and -41.2 % over the period within NA3. Interestingly, the median surface wind speeds in these seasons all project a decline. There is no evident trend within DJF surface winds (figure 12). This suggests a more turbulent future for the Rocky Mountain range within its current most turbulent season, but also a drop in the remaining three. Spring over this region, from climatology (Wolff and Sharman, 2008), can often have a peak in MWT similar to that in DJF. These results project a possible drop in this occurrence.

https://doi.org/10.5194/egusphere-2025-2378
Preprint. Discussion started: 27 June 2025

The last region in North America is NA5, which covers the southern states of the USA and the Caribbean. Within figure 1, it is evident that these southern USA states have pockets of MWT. However, once broken down into significant trends, these regions disappear. NA5 trends are therefore links purely to MWT over Haiti and the Dominican Republic. NA5 MWT rates were shown to decrease over the 101 years. These trends arose only in JJA, SON and MAM (figure 11) by -1.26 % , -0.59 % and -1.73 % over the entire period . This decrease is also linked to drops in median and maximum surface wind flow, but only for SON and MAM. JJA has a mix across two significant trends for median surface wind flow.

3.3.2 South America; SA1-SA3

There are three regions in South America shown in figure 10, that break down the Andes mountain range into northern (SA1), central (SA2) and southern (SA3) regions. Central and Southern Andes are projected to become considerably more turbulent, with amounts equal to and just greater than NA3. Northern and Central Andes projected MWT amounts are projected to decline within most GCMs for all seasons. The one outlier model and season in SA2 is EC-Earth-3P-HR's SON, which projects an increase within SH spring (figure 11.d) of +0.15 %/year. HadGEM3-GC3.1 projected decline is greater, and so on average projects a decline within DJF , JJA, MAM and SON by -11.6 % , -42.9 %, -25.8 % , -20.3 % and -11.6 % , respectively for SA2. There's high confidence that MWT will reduce, across all seasons, within SA1, with strong significant model agreement.

The Northern Andes MWT reduction is greatest in DJF by -22.3 %, then in MAM -16.0%, next SON -9.1% and finally JJA at -8.8% over 101 period. Interestingly, EC-Earth-3P-HR projected weaker surface median wind speed, across all seasons (if applicable). However, stronger surface maximum and median winds are evident in remaining GCMs. SA2's connection to surface wind speed is more apparent. SON's increase in EC-Earth-3P-HR could be linked to the slight stronger median surface winds. The decline in HadGEM3-GC3.1-HM, within this season, is possibly linked to stronger maximum wind speeds, but not median winds. Very similar results obtained for DJF. MAM has only one model with significant surface wind speed, it is in fact decreasing. However, surface winds in JJA are increasing, an opposite trend to how MWT is projected to shift in this area and season. This season has only one wind trend for comparison, but could suggest a seasonal dependence of MWT on low level wind speeds in this region.

There is variation in the GCM projections for the Southern Andes (SA3). Figure 10 projects a rise in MWT overall between the two decades, but only one GCM projects this rise (EC-Earth-3P-HR) and due to a wide range of index outcomes, has an insignificant slope. The remaining two GCMs project the opposite scenario with a decline in MWT frequency. These trends continue into the seasonal breakdown in figure 11 with HadGEM3-GC.1 and MPI-ESM1.2 project a drop in MWT across all seasons. A tug of war between an increase and decrease for each season arises with SON and MAM decreasing overall by -11/2% and -2.3% but DJF and JJA projections dominated by the single GCM (EC-Earth-3P-HR) with an average of +17.7% and +2.8% across all GCMs.

https://doi.org/10.5194/egusphere-2025-2378
Preprint. Discussion started: 27 June 2025

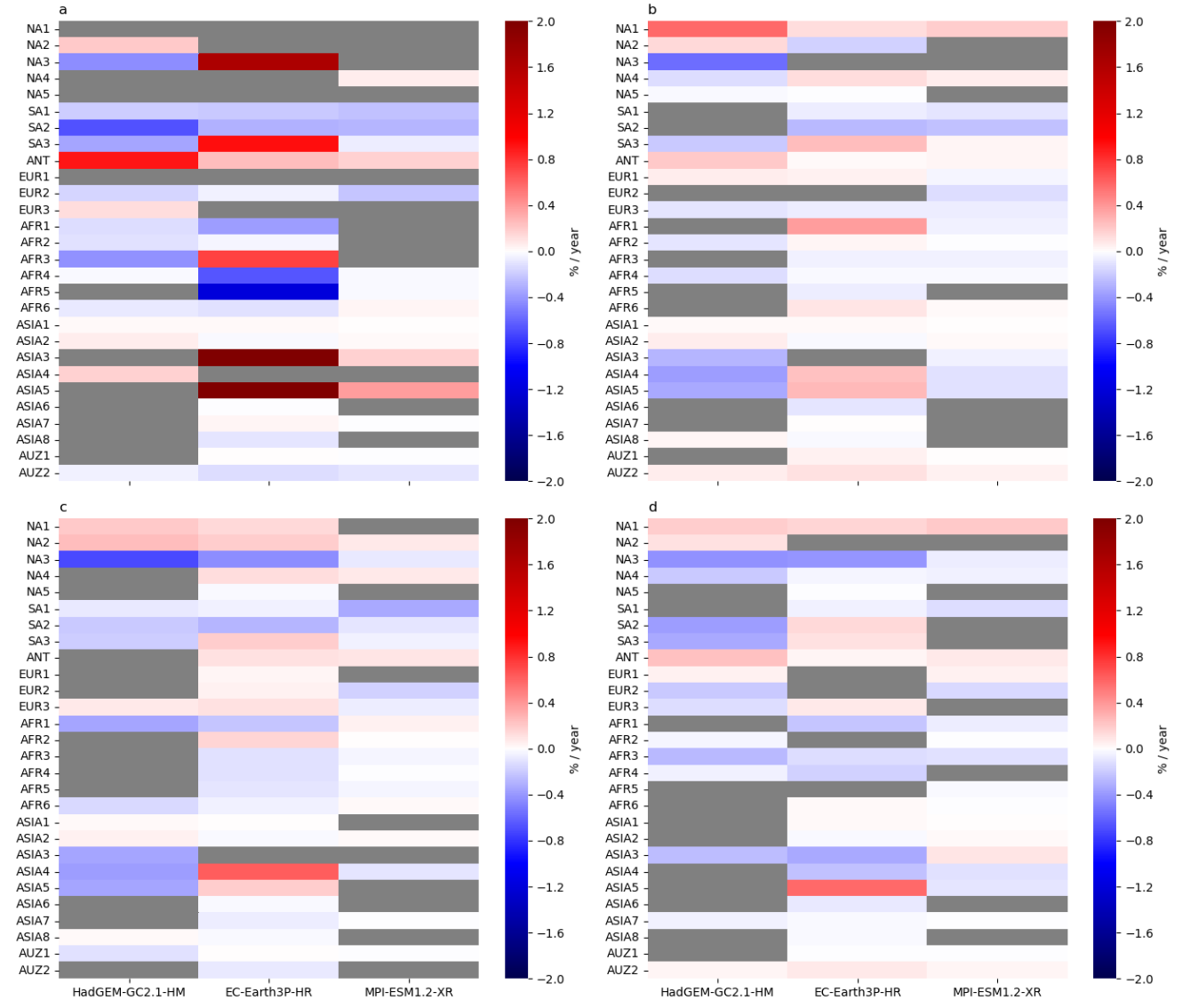

Figure 11. Seasonal trends for MWT over 28 sub-continental regions, highlighted in figure 10. Over the 101 year period, shaded grey if no significant trend. The figure breaks down results into columns associated with the three GCMs, as evident by labelling on the x-axis. DJF, JJA, MAM and SON displayed in subplot 'a','b','c' and 'd'.

https://doi.org/10.5194/egusphere-2025-2378
Preprint. Discussion started: 27 June 2025

Over North and South America, a trend has arisen with EC-Earth-3P-HR projections differing to MPI-ESM1.2-XR and HadGEM3-GC3.1-HM, usually with an opposing warming trend. This model variation is also evident within other continents. Within figure 12, SA3 has one significant trend, with a drop in median surface wind speeds with MAM HadGEM3-GC3.1-HM. This season and model projects a drop in MWT, suggesting a possible decline linked to low level wind speed.

3.3.3 Europe; EUR1-EUR3

There are three regions over Europe analysed in figure 10. It should be noted that EUR3 includes some areas in Africa and Asia. Similar to NA5, EUR3 had more patches of MWT in figure 1.g than figure 10, that have disappeared when considering the trends in time. figure 10 only shows the confident trends in MWT, rather than the existence of MWT. Figure 11 encapsulates differences across the seasons within this region. There's strong model agreement on a projected decrease in the amount of MWT by -8.1% in JJA within EUR3. HadGEM3-GC3.1-HM and MPI-ESM1.2-XR projections show a decline in both median and maximum surface wind speed. A decline in low-level wind speed, in both the median and max, are evident for the remaining seasons. In terms of MWT, SON overall decreased in frequency by -2.2% over the 101 period, despite a warming trend in EC-Earth-3P-HR projections. DJF and MAM are projected to increase on average by +13.9% and +4.4% over the century within EUR3.

In contrast, EUR1 and EUR2 have all seasons, in most GCMs, projecting an agreed upon trend in time. Despite, MPI-ESM1.2 projecting a slight drop in MWT in EUR1 summer rates, this season had an overall increase in MWT by +2.7%. Larger increase found in SON and MAM, with a percentage change of +5.1% and +4.4%. JJA and MAM MWT rise are consistent with stronger median surface winds (figure 12). DJF had no significant trends in time, so is shaded in grey within figure 11.a . EUR2 has all seasons projecting a decrease in MWT. There is quite strong confidence for a decline in DJF, with all three GCMs projecting a drop of -14.7% on average over the period. SON, JJA and MAM follow suit dropping by -18.3% , -13.1% and -6.5%. Interestingly, DJF and MAM have only one model each projecting a trend in figure 12. A decline in median surface wind speed is evident. EUR2, which encapsulated the Alps mountain range, is the most turbulent projected region of Europe. This projected decrease in such a turbulent region, will aid future flights through this busy continent.

3.3.4 Africa; AFR1-AFR6

Africa is split into six regions, with AFR1 slightly cutting off the bottom of Spain and Italy but primarily covering Morocco, Algeria, Tunisia and Libya. AFR1 is technically projected most turbulent region in Africa, bur AFR3 is a close second. AFR3 includes regions in the Middle East (Asia). AFR1 and AFR3 display a clear decline in MWT over our projected period of interest within figure 10. There are seasonal and model disagreements, evident in figure 11. Within AFR1, models agree on a decline with DJF, SON and mostly within MAM projections, with two out of three projecting a decline. Within JJA, EC-Earth-3P-HR projects a moderate increase (relative to the decrease projected

https://doi.org/10.5194/egusphere-2025-2378
Preprint. Discussion started: 27 June 2025

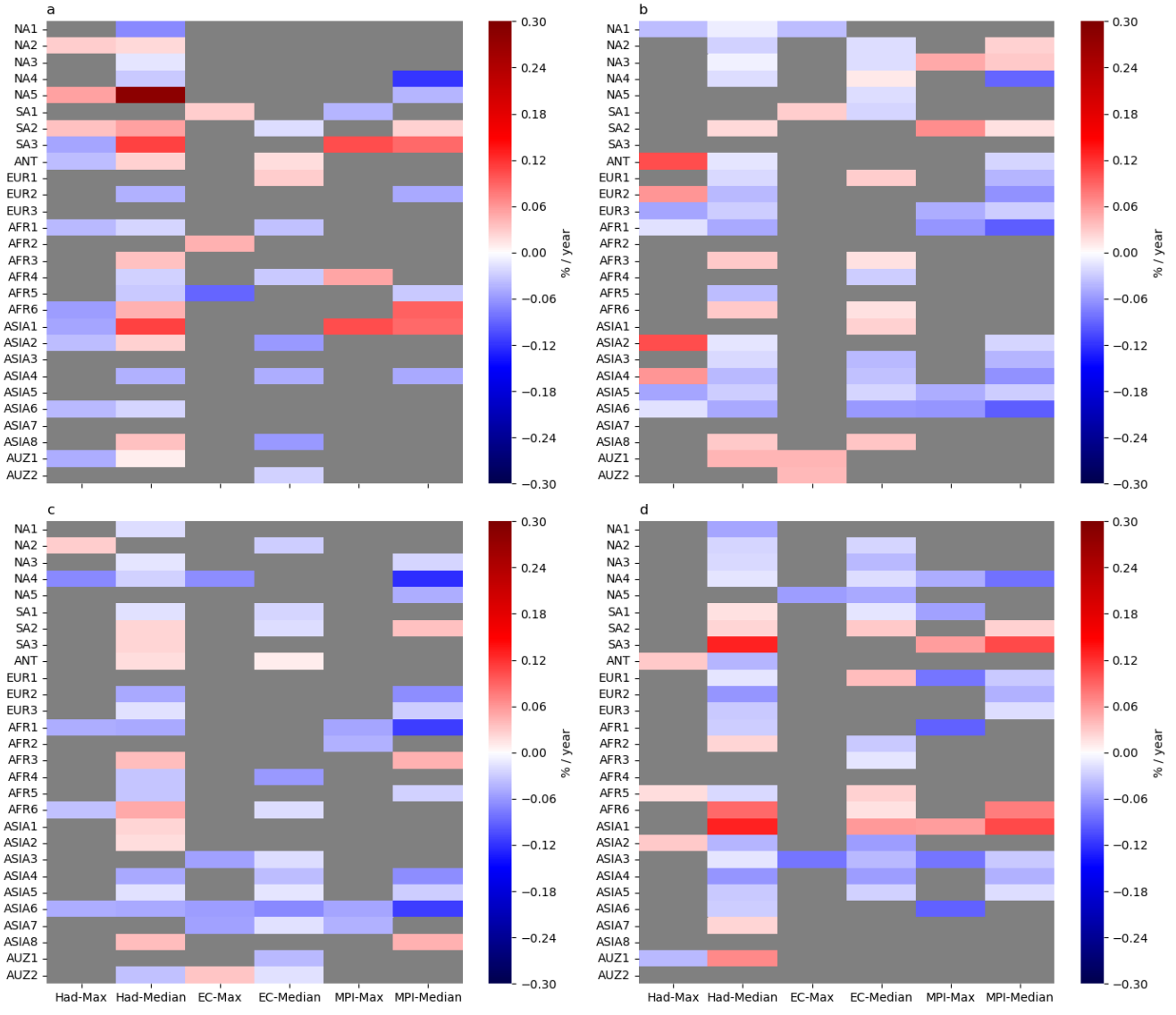

Figure 12. Trends in surface wind speed for each sub-region shown in figure 10. The Maximum and Median winds are discussed individually with notation 'Max' and 'Median' for all GCMs. Each model is donated similar to that in Table 1 & 2 with HadGEM3-GC3.1-HM referenced as 'Had', EC-Earth-3P-HR as 'EC' and MPI-ESM1.2-XR as 'MPI'. DJF, JJA, MAM and SON displayed in subplot 'a','b','c' and 'd'. The grey zones depict insignificant GCM projections.

https://doi.org/10.5194/egusphere-2025-2378
Preprint. Discussion started: 27 June 2025

by MPI-ESM1.2-XR) resulting in an overall average increase in +16.3 % over the 101 years. DJF, SON and MAM too project a moderate percentage change of -26.1% ,-15.2% and -17.6%. Median surface wind were found to weaken within these seasons (figure 12). Results for AFR3 are very similar to those for AFR1, but with an increase found in DJF. EC-Earth-3P-HR projects a steep slope of +0.75%/year. However, HadGEM3-GC3.1 projects a smaller yet still moderate slope of -0.4%/year. On average, AFR3 increase in DJF by +15.9% and decrease in MWT within JJA, SON and MAM by -5.8% , -16.9% and -7.9% . Interestingly, a mix of trends arose for surface wind flow in JJA. The decreases in MAM and SON MWT results are consistent with the decrease seen in low-level median wind flow.

AFR2, AFR4, AFR5 and AFR6 have a much smaller amount of MWT compared to AFR1 and AFR3, this is shown by the negative values the scatter remains in with figure 10. In general a decrease in MWT projected across these areas. However, EC-Earth-3P-HR project a notable increase in AFR2 and ARF6 within figure 11. This leads to an overall increase of +8.5% in MAM within AFR2 and +6.2% in JJA in AFR6. This summer increase is linked to stronger median surface winds in this model (figure 12). However, within AFR2, all surface wind speed changes are projected to get stronger in DJF yet MWT rates are dropping by -7.5%. Despite median surface wind trend often associated with the corresponding trend in MWT, there are a few exceptions with differing outcomes. JJA and SON project a slight decrease in MWT of -0. 5% and -1. 9%. AFR6 has a slight increase in SON by +1.1%, but declines in DJF and MAM by -9.2% and -4.9% over the 101 year period. The most considerable decrease in Africa are found within AFR5, with DJF MWT rates decreasing by -61.6% over the 101 year period. EC-Earth-3P-HR is the considerable driver in these large trends (figure 11.a). A decrease in MWT also evident in JJA, SON and MAM, with strong model agreement, but at lower rates of -6.8%, -2.20% and -6.6% for AFR5. The change in maximum wind speed decrease in all seasons within ARF5, correlating to the MWT trend. AFR4 has its most notable decrease in MWT within SON by -12.0 %, followed by MAM by -6.4% and then similar declines in MWT within DJF and JJA on average across the GCMs at -2.4% and -2.3%.

3.3.5 Asia; ASIA1-ASIA8

Over Asia, eight zones were chosen for further analysis. This was done due to differing trends on initial analysis and MWT developing in many regions over this continent. The largest amount of projected MWT is found in Asia in zone ASIA4. This area includes the Himalayan mountain range and Tibetan plateau within it. As figure 10 clearly shows, this area is decreasing in percentage of MWT by the end of the century compared to the beginning. However, figure 11, shows this decline is only evident in SON, with two significant slopes in models EC-Earth-3P and MPI-ESM1.2-XR projecting a drop of -18.4% on average over the period. This is linked to weaker median surface winds this season, as evident in figure 12. Within ASIS4, both JJA and MAM have HadGEM3-GC3.1-HM and MPI-ESM1.2-XR models projecting a decline in MWT, with EC-Earth-3P-HR projecting a considerable increase. In the tug of war, EC-Earth-3P monopolizes MAM projections due to its steep slope of +0.64 %/year. This leaves ASIA4 increase on average of +5.0% in MAM. The other two GCMs dominate the JJA averages, resulting in an overall decrease

https://doi.org/10.5194/egusphere-2025-2378
Preprint. Discussion started: 27 June 2025

of -8.5% over 101 years. HadGEM3-GC3.1-HM, despite projecting a decrease in JJA, projected stronger maximum surface winds but weaker median surface wind flow. Interestingly, EC-Earth-3P-HR MAM median surface winds projected a rise over the 101-year period, a different trend to that examined above around MWT percentage shifts. Only HadGEM3-GC3.1 projects significant slopes in DJF, with a projected increase of 18.3%. One can note an almost equal shift in MWT across seasons from SON towards DJF. This level of increase within the most turbulent projected region of the globe is a noteworthy finding, considering that long-haul flights often travel through this area. The median surface wind flow projecting a decline over DJF within figure 12, suggests this increase is possibly linked to upper-level dynamical variation. The strengthening in upper-level jet streams in time has lead to an increase in clear air turbulence production. As projected MWT has large seasonal shifts throughout the globe, perhaps alterations in the upper-level jet with climate change is also having a direct or in-direct impact on MWT production. Further research should be done on this possible connection.

ASIA5 and ASIA3 are the 2nd and 3rd most turbulent regions in the Asia. ASIA3 interestingly, within figure 10, has two significant slopes both projecting different trends in time. These two opposing trends arise from averaging over a large region and seasonal variation. EC-Earth-3P-HR is not within this scatter plot but has significant trends when broken down seasonally, with a DJF trend of +2.0%/year. DJF, averaged over GCMs, has an increase of +112.3% in MOG MWT over this region. Fascinatingly, the remaining seasonal project an overall decrease in MOG MWT, by -36.1 % (MAM), -17.4% (JJA) and -16.6% (SON). A trend also evident this regions median and maximum surface winds (figure 12). No significant surface wind trends found for DJF in AISA3 or ASIS5. However, there are significant MOG MWT within DJF in ASIA5, with an increase of +123.4%. SON also projected an overall average change of +23.0%. A decrease was found in JJA and MAM by -5.9% and -7.9%. In relation to surface wind speeds trends, this region had JJA, MAM and SON all with projected declines in median and maximum.

The remaining regions in Asia propagate below zero in figure 10 scatter plots, and therefore have considerable less MWT amounts than the three aforementioned ASIA zones. Within figure 11, ASIA2 EC-Earth-3P-HR projects a decline in MWT over all seasons in this region, possibly associated with the slight drop over southern Japan (figure 10). The remaining two GCMs, if applicable, projected an increase in MWT in all seasons. This is further evident in figure 10 ASIA2 side plot, with MPI-ESM1.2 and HadGEM3-GC3.1 projecting an increase, but EC-Earth-3P-HR projecting a decline. Overall the maximum increase in this region arose in JJA at +2.4% in JJA and minimum in SON of +0.8% over the 101 years. ASIA1, has a slight increase across all GCMs (strong model agreement) and seasons, with the maximum percentage change over the century at +1.7% in SON and minimum of +1.4% in DJF.

The final three regions of Asia encompass Indian and Sri Lanka (ASIA6), south eastern Asia (ASIA7/8) and a few countries in the Australian continent (Papa New Guinea; ASIA8). ASIA6-8 have a general decline over the period, with a decrease in SON and MAM. Although a slight MAM increase in HadGEM3-GC3.1 in ASIA8. IN DJF, ASIA6 projects extremely small increase over the 101 years (-0.08%) , ASIA7 projects a light increase (1.86%),

https://doi.org/10.5194/egusphere-2025-2378
Preprint. Discussion started: 27 June 2025

with ASIA8 finding a decline in MWT of -10.1% . Within the JJA projections, ASIA6 has a relatively moderate decline of -9.9% , ASIA7 projects slight increase of +0.5% and ASIA8 has two disagreeing GCMs projecting a slight increase (HadGEM3-GC3.1-HM) and decrease (EC-Earth-3P) overall resulting in a small increase of +0.76% over the century.

3.3.6 Australia and Antarctic; AUZ1, AUZ2 and ANT

As discussed there are technically three regions within the Australian continents. AUZ1 and AUZ2 are located south of ASI8 over Australia and New Zealand. AUZ1, which includes areas in the Australian country like New South Wales, Victoria and Tasmania, had more features within figure 1, but only a few scattered patches within figure 10's global map. The lines within AUZ1's scatter plot both project an overall slight decrease over the 101 years. Within figure 11, the white patches occur often in subplots a,b,c and d within the AUZ1 section. They suggest an extremely small, almost no change result. However, in MAM and JJA, there are slight shifts within HadGEM3-GC3.1 and EC-Earth-3P results with a decrease of -3.8% in MAM and increase of +1.6% in JJA over the 101 year projected period. These trends correlate to shifts in low-level surface wind speed shifts within the period. AUZ2, which covers New Zealand, looks to be increasing in time within figure 10 . SH winter and spring (JJA, SON) have full model agreed projected positively sloped trends in time, increasing by +8.4% and +5.9% over the period. However, DJF (SH summer) and MAM (SH autumn) are decreasing in time, with GCMs agreement, by -9.4% and -8.1% . Interestingly, the amount of MWT in this box is greater than many regions in Asia and Africa.

There are no new regions in the Antarctic, with similar projections evident across continent. However, the scatter box, titled 'ANT' do show the average over the previous line plots in figure 9 . The average amount of MWT over the Antarctic, across the indices, is just greater than the Alps (EUR2) and around a similar range as found in AFR1 over the Atlas Mountains. The increases here correlate to the findings in Table 2, with an steep increase found in DJF, particularly in HadGEM3-GC3.1 model. This shift may partly be associated with increased low-level and upper-level wind speed over this polar region. The British Antarctic Survey found surface winds strengthen by 15% since 1980. This is a trend evident in figure A.1 to 5 and within figure 12, with all GCMs and both median and maximum surface wind trends projecting stronger flow for the Antarctic continent.

4 Conclusions

Through the use of three HighRes-MIP CMIP6 GCMs, this study investigates the modeled projections of global MWT turbulence over a 101-year period. Through an initial comparison between the 1950-60 and 2040-50 decade, one found coarser models were not able to detect as much detail as their finer counterparts. This was linked to improved gradient and terrain height information. This study continued only with three higher resolution models; HadGEM3-GC3.1-HM (25km), EC-Earth-3P-HR(36km) and MPI-ESM1.2-XR (34km). Each MWT index was broken down and

https://doi.org/10.5194/egusphere-2025-2378
Preprint. Discussion started: 27 June 2025

analysed initially through continental yearly analysis (figure 3 to 9). Regional dependencies arose around model and index agreement, with seasonal components an important contributor to results. Finally a sub-regional approach was discussed, where seasonal MWT and surface wind speed trends were analysed.

On average, the North American continent had an increase in MWT since the starting decade. However, a lot of the trends in time were not deemed significant. On further sub-continental analysis, the zone encapsulating the Rocky Mountain range, was shown to be decreasing in the amount of MWT in all seasons but NH winter. Within DJF, increase of +60.6% in MOG MWT arose, with similar yet opposite rates of -58.3%, -41.2 % and -30.9% for JJA, MAM and SON. Greenland, a region used often for transatlantic travel, is increasing in the amount of MWT, with its greatest shift in JJA by +30.5%. Over South America, a decrease in MWT was evident from initial analysis. There is strong model agreement that the North and Central regions of the Andes will have a large decreases in MOG MWT within SH summer (DJF), with drops of -22.3% and -49.2%, retrospectively. Southern Andes have a shift across seasons, with DJF and JJA projecting increases in MWT, at most in DJF at +17.7%. Although SON and MAM, project a decline, at most at -11.2% in SON.

Over Europe and Africa, a decline in MWT is evident over the Alps and Atlas Mountain ranges. NH autumn over the Alps has the largest decline of -18.3%, followed quickly after by DJF at -14.7%. DJF had a decline of -26.1% over parts of the Atlas mountains, with a decline in MWT evident across the entire African continent. However, large increases arose over Asia, with two regions projected an increase above +100% (ASIA3/5) in DJF. Interestingly, over the Tibetan plateau and Himalayas, MWT rates increased within DJF and MAM by +18.3% and +5.0%, but a similar yet opposite increase for SON and JJA of -18.4% and -8.5%. The last region of significant change occurred over the Antarctica peninsular, with DJF and JJA increasing by +32% and +8.7%. Further regions were explored, with many areas having a close trend related to median surface wind speed and it change over the century. However, several regions and seasons were less dependent on the low-level wind speeds. In terms of significance to forecasting operations in the aviation sector, results over Asia, Europe, North and South America are key, considering the high density of flights that travel over these regions.

Overall, a mixture of MWT changes arose across the globe. The aviation sector should be aware of the future projections in MWT, particularly for those were large increase over the 101 year period were evident, such as Asia, Greenland and the Antarctic. Future work should focus on differing warming scenarios, other to SSP5-8.5, to get a full picture of possible future MWT outcomes.

4.1 Limitations

This paper acknowledges that modelled atmospheric and ocean data is used, all projections are based on a future scenario of the globe.SSP5-8.5 is the extreme climate warming scenario with no action, with little mitigation or adaptation (Deng 2022). One limitation within previous work (Sharman and Pearsons (2017), Kim et al. (2023), that

https://doi.org/10.5194/egusphere-2025-2378
Preprint. Discussion started: 27 June 2025

continues within this paper is that MWT often occurs downstream from mountain ranges (Wilms,Henrike,20220). Our region should encapsulate source of the downstream MWT due to our inclusion of slope gradient, but may miss MWT which travels far distances due to certain meteorological conditions (Lane et. al, 2009).

Appendix A: Breakdown into Indices; Two decadal comparison

Figure A.1, A.2 and A.3 display the decade difference for HadGEM3-GC3.1-HM, EC-Earth-3P-HR and MPI-ESM1.2-XR individually, for each index, rather than averaged (figure 2). These figures also include the decade difference in daily maximum (g) and median (h) surface wind speeds. As mentioned in Section 2.0; Methodology and Data, low-level wind speed is a variable within our MWT indices. One area of investigation is to understand if a shift in MWT is linked to possible changes in surface winds. Deng et al. (2022), using different, coarser CMIP6 GCMs and observational data, found CMIP6 GCMs correctly reproduced the decreasing trends (between 1980-2010 and 2070-99) in near surface winds in North America, Europe and East Asia. They did on average simulate faster wind speeds at coastal areas than inland, and have shown seasonal variations. Please note these wind speed percentage change only displays results over regions in which MWT arises, other areas excluded for ease of comparison.

Within the HadGEM3-GC3.1-HM (25km) model, a general increase in maximum wind speed is apparent in figure A.1.g, with a larger percentage change compared to the change in average surface wind speed (figure A.1.h). The maximum surface winds have relatively large percentage shifts over Greenland, the Antarctic and Asia. These regional increases correlate the rise in MWT frequency in many indices within this figure. Interestingly, average wind speed has more regions that project decrease over the continents, than maximum wind speed, particularly interesting is the decline on the coastlines of the Antarctic between 60-180 °E. One could argue the changes in wind speed, in both maximum and average, correlate to projected MWT percentage differences in such indices as MWT_{FD}, MWT_{FDWS},MWT_{WS}. Within this figure, the projected outcomes from these indices are relative similar within the HadGEM3-GC3.1-HM model.

Interestingly, MWT_{DIV} (figure A.1c) projects a very notable MWT decline across the globe, including southern Greenland, the North America Rocky, Central and Southern Andes and the Himalayas. A decline in maximum wind speeds arises over the Antarctic and north west Greenland, regions where MWT_{DIV} projects a drop in MWT frequency between the two decades. MWT_{HTG} (figure A.1a) is an index shown to effectively represent MWT over North America, according to ROC curve analysis from Shaman and Pearson's (2017). This index projects either no change or a decline in MWT over southern Greenland, USA and Canada. Despite similarities to MWT_{DIV}, MWT_{HTG} differs over the African and Asian contentment, with an increase in turbulence at the southern edge of the Tibetan Plateau. The most notable index within figure A.1 is MWT_{FF}, with a pronounced decline projected over the northern Andes, eastern Africa, the Himalayas and Indonesia and a substantial increase projected in other regions of the globe. Except for similarities in North America, MWT_{FF} and MWT_{HTG} have almost opposite projections.

https://doi.org/10.5194/egusphere-2025-2378
Preprint. Discussion started: 27 June 2025

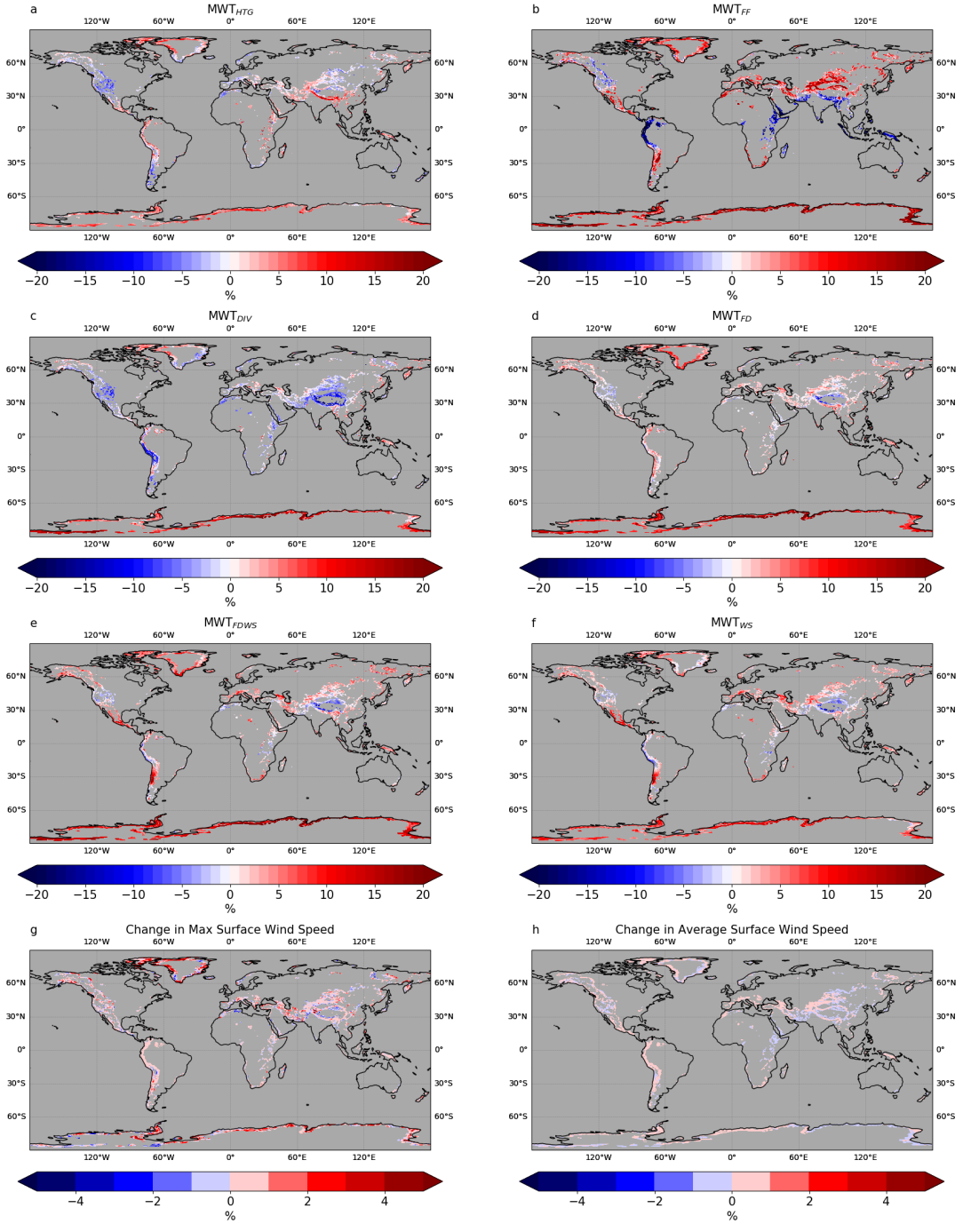

Figure A1. The decade percentage difference in MWT between 1950-59 and 2040-49, for the six MWT indices using the Met. Office Model HadGEM3-GC3.1-HM with grid spacing domain of 25km, averaged over three ensemble member runs (a-f). The change in maximum and median wind speed, between these two previous mentioned decades, within HadGEM3-GC3.1-HM is highlighted in subplots g and h respectively.

https://doi.org/10.5194/egusphere-2025-2378
Preprint. Discussion started: 27 June 2025

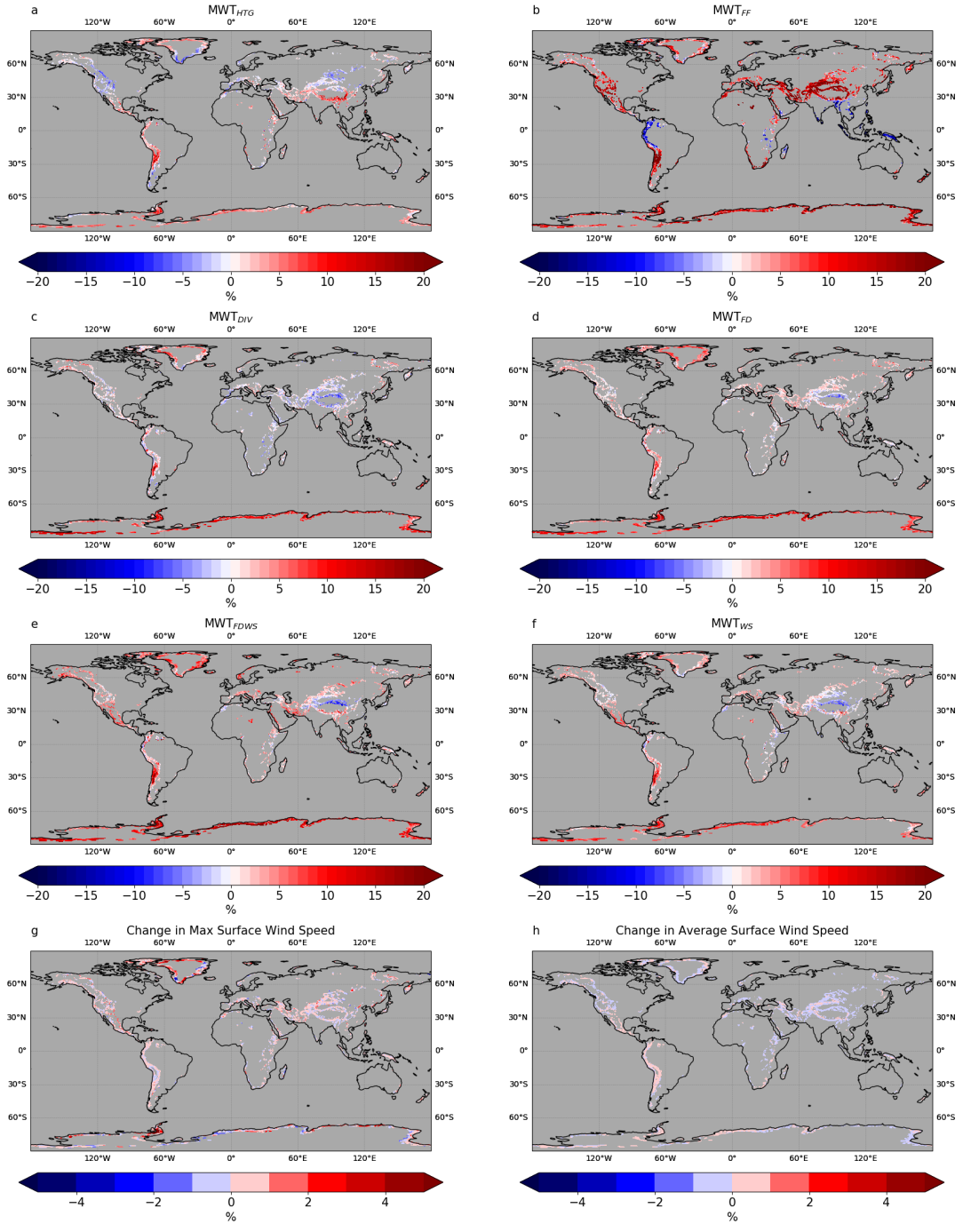

Figure A2. The decade percentage difference in MWT between 11950-59 and 2040-49, for the six MWT indices using EC-Earth-3P-HR with grid spacing domain of 36km, averaged over two ensemble member runs.

https://doi.org/10.5194/egusphere-2025-2378
Preprint. Discussion started: 27 June 2025

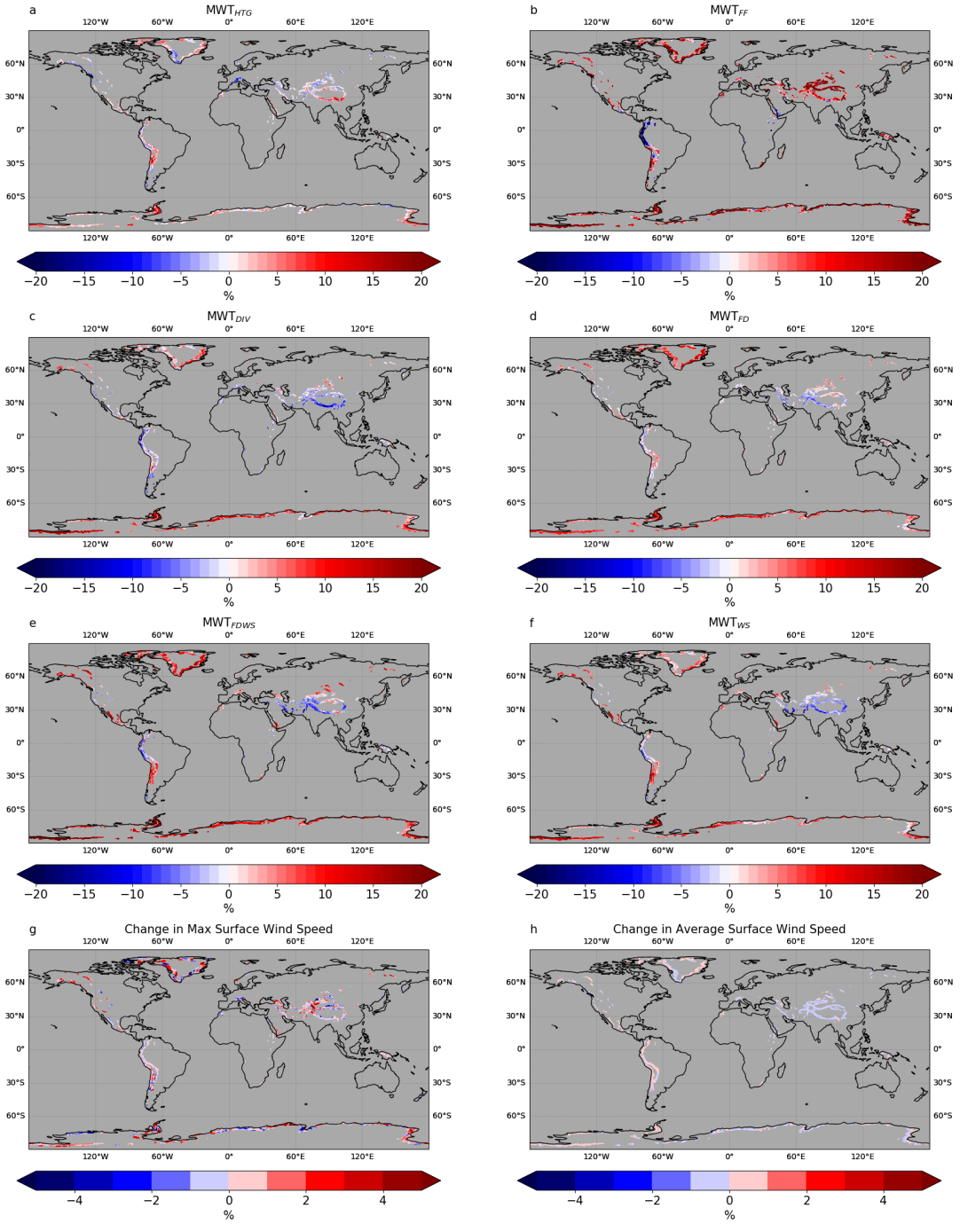

Figure A3. The decade percentage difference in MWT between 1950 and 2040-49 (2040-49-1950) for the six MWT indices using Max-Planck Institute GCM MPI-ESM1.2-XR with grid spacing domain of 34km.

https://doi.org/10.5194/egusphere-2025-2378
Preprint. Discussion started: 27 June 2025

The EC-Earth-3P-HR (36km) and MPI-ESM1.2-XR (34km) too have the most notable change found within MWT_{FF}. These two models project a greater overall increase over Asia than HadGEM3-GC3.1-HM within this index. There is a notable drop in the number of regions producing MWT within MPI-ESM1.2-XR projections. However, in comparison to the mid-range and coarser models, a large percentage of the globe is still incorporated. MWT_{DIV} within figure A.3 projects a similar decrease to that evident in HadGEM3-GC3.1-HM (figure A.1c) results, over the regions available. Interestingly, EC-Earth-3P-HR projects a decrease in some regions, using MWT_{DIV}, but a much smaller percentage change. In some cases MWT_{DIV} project a slight increase in areas which decreased in figure A.1 (North/South America). Despite these difference, these spatial maps from figure A.1 to 5 suggest a greater variation in trends in the indices than GCMs.

The change in surface wind speed marginally differs across the GCMs. Although, EC-Earth-3P-HR compared to HadGEM3-GC3.1-HM projects weaker winds inland over Asia, Greenland and North America, for change in average wind speeds. MPI-ESM1.2-XR also projects weaker winds over Asia within figure A.3 (h). These differences highlight the impact of the average surface wind on MWT_{FD}, MWT_{FDWS}, MWT_{WS} projections. These weaker winds link to negative changes in MWT, particularly over Asia.

https://doi.org/10.5194/egusphere-2025-2378
Preprint. Discussion started: 27 June 2025

References

Deng, K., Liu, W., Azorin-Molina, C., Yang, S., Li, H., Zhang, G., et al. (2022). Terrestrial stilling projected to continue in the Northern Hemisphere mid-latitudes. *Earth's Future*, 10, e2021EF002448. https://doi.org/10.1029/2021EF002448

Gill, P. G., Stirling, A. J. (2013). Including convection in global turbulence forecasts. *Meteorol. Appl.*, 20(1), 107–114. https://doi.org/10.1002/met.1315

Haarsma, R., Roberts, M., Vidale, P., Senior, C., Bellucci, A., Bao, Q., Chang, P., Corti, S., Fučkar, N., Guemas, V., von Hardenberg, J., Hazeleger, W., Kodama, C., Koenigk, T., Leung, L., Lu, J., Luo, J., Mao, J., Mizielinski, M., Mizuta, R., Nobre, P., Satoh, M., Scoccimarro, E., Semmler, T., Small, J., von Storch, J. (2016). High resolution model intercomparison project (HighResMIP v1.0) for CMIP6. *Geosci Model Dev*, 9(11), 4185–4208. https://doi.org/10.5194/gmd-9-4185-2016

Kim, J., Sharman, R., Strahan, M., Scheck, J., Bartholomew, C., Cheung, J., Gait, N. (2018). Improvements in Nonconvective Aviation Turbulence Prediction for the World Area Forecast System. *Bulletin of the American Meteorological Society*, 99(11), 2295–2311. https://doi.org/10.1175/bams-d-17-0117.1

Kim, S., Kim, J., Chun, H., Sharman, R. D. (2023). Global response of upper-level aviation turbulence from various sources to climate change. *npj Climate and Atmospheric Science*, 6(1), 92. https://doi.org/10.1038/s41612-023-00421-3

Lane, T., Doyle, J., Sharman, R. D., Shapiro, M. A., Watson, C. D. (2009). Statistics and dynamics of aircraft encounters of turbulence over Greenland. *Monthly Weather Review*, 137(8), 2687–2702. https://doi.org/10.1175/2009MWR2878.1

Lester, P. F. (1993). Turbulence: A New Perspective for Pilots. Jappesen Sanderson, Englewood, CO.

Prosser, M. C., Williams, P. D., Marlton, G. J., Harrison, R. G. (2023). Evidence for large increases in clear-air turbulence over the past four decades. *Geophysical Research Letters*, 50, e2023GL103814. https://doi.org/10.1029/2023GL103814

Sharman, R., Tebaldi, C., Wiener, G., Wolff, J. (2006). An integrated approach to mid- and upper-level turbulence forecasting. *Weather and Forecasting*, 21, 268–287. https://doi.org/10.1175/WAF924.1

Sharman, R. D., et al. (2014). Description and derived climatologies of automated in situ eddy-dissipation-rate reports of atmospheric turbulence. *J Appl Meteorol Climatol*, 53(6), 1416–1432. https://doi.org/10.1175/JAMC-D-13-0329.1

Sharman, R., Lane, T. (2016). Aviation Turbulence: Processes, Detection, Prediction. Springer International Publishing. https://doi.org/10.1007/978-3-319-23630-8

Sharman, R., Pearsons, J. M. (2017). Prediction of energy dissipation rates for aviation turbulence. Part I: Forecasting nonconvective turbulence. *Journal of Applied Meteorology and Climatology*, 56(2), 317–337. https://doi.org/10.1175/JAMC-D-16-0205.1

Smith, I. H., Williams, P. D., Schiemann, R. (2023). Clear-air turbulence trends over the North Atlantic in high-resolution climate models. *Clim Dyn*. https://doi.org/10.1007/s00382-023-06694-x

Storer, L. N., Williams, P. D., Joshi, M. M. (2017). Global response of clear-air turbulence to climate change. *Geophys Res Lett*, 44(19), 9976–9984. https://doi.org/10.1002/2017GL074618

Whiteway, J. A., Pavelin, E. G., Busen, R., Hacker, J., Vosper, S. (2003). Airborne measurements of gravity wave breaking at the tropopause. *Geophysical Research Letters*, 30(20). https://doi.org/10.1029/2003GL018207

Williams, P. D. (2017). Increased light, moderate, and severe clear-air turbulence in response to climate change. *Adv Atmos Sci*, 34(5), 576–586. https://doi.org/10.1007/s00376-017-6268-2

https://doi.org/10.5194/egusphere-2025-2378
Preprint. Discussion started: 27 June 2025

Williams, P. D., Joshi, M. M. (2013). Intensification of winter transatlantic aviation turbulence in response to climate change. *Nat Clim Chang*, 3(7), 644–648. https://doi.org/10.1038/nclimate1866

Williams, P. D., Storer, L. N. (2022). Can a climate model successfully diagnose clear-air turbulence and its response to climate change? *Q J R Meteorol Soc*, 148(744), 1424–1438. https://doi.org/10.1002/qj.4270

Wolff, J., Sharman, R. D. (2008). Climatology of upper-level turbulence over the contiguous United States. *Journal of Applied Meteorology and Climatology*, 47(8), 2198–2214. https://doi.org/10.1175/2008JAMC1799.1

Zeng, Z., Ziegler, A., Searchinger, T., Yang, L., Chen, A., Ju, K., Piao, S., Li, L., Ciais, P., Chen, D., Liu, J., Azorin-Molina, C., Chappell, A., Medvigy, D., Wood, E. (2019). A reversal in global terrestrial stilling and its implications for wind energy production. *Nature Climate Change*, 9(12), 979–985. https://doi.org/10.1038/s41558-019-0622-6

Acknowledgements. We would like to acknowledge and thank the Natural Environmental Research Council (NERC) for funding the research project which lead to this publication. We acknowledge the World Climate Research Programme, which, through its Working Group on Coupled Modelling, coordinated and promoted CMIP6. Within this we thank the CMIP6 endorsement of the High-Resolution Model Intercomparison Project (HighResMIP). We thank the climate modelling groups for producing and making available their model output, and the multiple funding agencies who support CMIP6. The authors would like to also acknowledge and thank the UKRI funded JASMIN data analysis facility, needed for storage and analysis of the PRIMAVERA (Process-Based Climate Simulation: Advances in High Resolution Modelling and European Climate Risk Assessment: https:// www. prima vera- h2020. eu/) project data.

Author contributions. IHS: conceptualization, Formal analysis, inves- tigation, project administration, software, visualization, writing— original draft, writing—review and editing. PDW: conceptualization, funding acquisition, methodology, project administration, supervision, writing—review and editing. RS: conceptualization, funding acqui- sition, methodology, project administration, supervision, writing— review and editing.

Competing interests. The authors of this paper have no relevant financial or non-financial interests to disclose.

Code availability. Available on request

Data availability. To access the Coupled Model Inter-comparison Project phase 6 (CMIP6) global climate model data, via the same routes as the authors, please contact PRIAMVERA partners from https://www.primavera-h2020.eu/. The PRIMAVERA project is led by the Met Office and the University of Reading.